

WANL-PR(Q)-011
NASA-CR-72093

DEVELOPMENT OF DISPERSION STRENGTHENED TANTALUM BASE ALLOY

Tenth Quarterly Report

by

R. W. Buckman and R. C. Goodspeed

prepared for

National Aeronautics and Space Administration

Lewis Research Center

Space Power Systems Division

Under Contract (NAS 3-2542)



**ASTRONUCLEAR LABORATORY
WESTINGHOUSE ELECTRIC CORPORATION**

Facility Form 602

N67-39575
(ACCESSION NUMBER)

10705225
(PAGES)

Q# 72093
(NASA CR OR TXN OR AD NUMBER)

(THRU)

(CODE)

17
(CATEGORY)

NOTICE

This report was prepared as an account of Government-sponsored work. Neither the United States nor the National Aeronautics and Space Administration (NASA), nor any person acting on behalf of NASA:

- A) Makes any warranty or representation, expressed or implied, with respect to the accuracy, completeness, or usefulness of the information contained in this report, or that the use of any information, apparatus, method, or process disclosed in this report may not infringe privately-owned rights; or
- B) Assumes any liabilities with respect to the use of, or for damages resulting from the use of any information, apparatus, method or process disclosed in this report.

As used above, "person acting on behalf of NASA" includes any employee or contractor of NASA, or employee of such contractor, to the extent that such employee or contractor of NASA or employee of such contractor prepares, disseminates, or provides access to, any information pursuant to his employment or contract with NASA, or his employment with such contractor.

Copies of this report can be obtained from:

National Aeronautics & Space Administration
Office of Scientific and Technical Information
Washington 25, D. C.
Attention: AFSS-A

3 DEVELOPMENT OF DISPERSION STRENGTHENED
TANTALUM BASE ALLOY 4

QPR-10. and

by

6 R. W. Buckman, Jr.

and

R. C. Goodspeed 7

4 TENTH QUARTERLY PROGRESS REPORT 4a

Covering the Period

14 February 20, 1966 to May 20, 1966 6L1001

Prepared For

NATIONAL AERONAUTICS AND SPACE ADMINISTRATION

15 Contract NAS 3-2542 29

Technical Management
Paul E. Moorhead
NASA-Lewis Research Center
Space Power Systems Division

Astronuclear Laboratory. 3
1 Westinghouse Electric Corporation
Pittsburgh 36, Pa. 2

ABSTRACT

Development of dispersion strengthened tantalum base alloys for use in advanced space power systems continued with the evaluation of oxygen contaminated and welded compositions which had been aged 1000 hours at 1800°F. The six **alloys** evaluated included carbide, nitride, and carbonitride strengthened types as well as two solid solution alloys. The effect of final annealing temperature on the creep behavior and room temperature mechanical properties of Ta-8W-1Re-0.7Hf-0.025C (ASTAR-811C) was investigated. The compositions of the remaining two four-inch diameter scale-up ingots were tentatively selected.

TABLE OF CONTENTS

	<u>Page No.</u>
I. INTRODUCTION	1
II. PROGRAM STATUS	3
A. WELDABILITY AND THERMAL STABILITY STUDY	3
B. SCALE-UP INVESTIGATION	25
C. PHASE IDENTIFICATION AND MORPHOLOGY	45
III. FUTURE WORK	45
IV. REFERENCES	46
APPENDIX I	48

LIST OF FIGURES

	<u>Page No.</u>
1. Comparison of Weight Gain Versus Chemical Analyses Determinations of Oxygen Contaminated Tantalum Alloy Samples	6
2. Effect of Maximum Weld Specimen Hardness on Ductile-Brittle Transition Temperature	9
3. Diamond Pyramid Hardness Traverses of NASV-21 Weld Specimens	11
4. Microstructures of NASV-21 Welded Specimens	12
5. Diamond Pyramid Hardness Traverses of ASTAR-81 1C Weld Specimens	13
6. Microstructures of ASTAR-81 1C Welded Specimens	14
7. Diamond Pyramid Hardness Traverses of NASV-18 Weld Specimens	16
8. Microstructures of NASV-18 Welded Specimens	17
9. Diamond Pyramid Hardness Traverses of NASV-12 Weld Specimens	19
10. Microstructures of NASV-12 Welded Specimens	20
11. Effect of Grain Size on Creep Rate of ASTAR-81 1C at 2400°F	31
12. Creep Behavior of Ta-8W-1Re-0.7Hf-0.025C(ASTAR-81 1C)	33
13. Room Temperature Mechanical Properties of NASV-20 as a Function of Heat Treatment	36
14. Macro and Microstructure of R. T. Tensile Specimens of NASV-20 Annealed for 1 Hour at 1650,1800,2000, and 2200°C Respectively Prior to Testing	37
15. Macro and Microstructure of TIG Welded Tensile Specimens of NASV-20	40
16. Microstructure of TIG Welded Specimens of NASV-20 Tested at -320°F, Showing Mechanical Twinning	41

LIST OF FIGURES (CONTINUED)

		<u>Page No.</u>
17.	Macro and Microstructure of TIG Welded Tensile Specimens of NASV-20	43
18.	Microstructure of TIG Welded Tensile Specimens of NASV-20 Tested at Elevated Temperature	44

LIST OF TABLES

		<u>Page No.</u>
1.	Oxygen and Carbon Contamination Data of Intentionally Oxygen-Contaminated Sheet	5
2.	Ductile-Brittle Transition Temperature Results of Weldability and Thermal Stability Study	7
3.	Effect of 1000 Hours at 1800°F on the Hardness of Tantalum Alloy Sheet	10
4.	Hardness of Oxygen Contaminated Tantalum Alloys Before and After Exposing for 1000 Hours at 1800°F	23
5.	Ductile-Brittle Transition Temperature of ASTAR-811C in As-TIG Welded Condition	26
6.	Room Temperature Hardness, Microstructure, and Grain Size of As-Rolled ASTAR-811C (NASV-20) Sheet After Annealing for 1 Hour at Temperature	27
7.	Mechanical Properties of ASTAR-811C (Heat NASV-20)	28
8.	Creep Results on ASTAR-811C	30
9.	Room Temperature Mechanical Properties of ASTAR-811C as a Function of Pre-Test Heat Treatment	35
10.	Tensile Properties of TIG Welded ASTAR-811C	39

I. INTRODUCTION

This, the tenth quarterly progress report on the NASA-sponsored program "Development of a Dispersion Strengthened Tantalum Base Alloy", describes the work accomplished during the period February 20, 1966 to May 20, 1966. The work was performed under Contract NAS 3-2542.

The primary objective of this Phase II work is the double vacuum arc melting of three compositions in the form of 60-pound, 4-inch diameter ingots. These compositions, which are to be used for sheet and tubing applications, will be selected for their weldability, creep resistance, and fabricability characteristics.

Prior to this quarterly period several promising tantalum alloy compositions were developed. These alloys exhibited good creep resistance at temperatures up to 1315°C (2400°F) while maintaining adequate fabricability and weldability. From these alloys a weldable composition containing a carbide dispersion, ASTAR-811C (Ta-8W-1Re-0.7Hf-0.025C) was selected and melted as the first 4-inch diameter ingot (Heat NASV-20). One section of this ingot was upset forged and another was side forged. Both forgings were processed to 0.04-inch sheet and detailed processing information was compiled. Evaluation of this sheet has been essentially completed.

During this quarterly period, the 1000-hour, 1800°F isothermal anneal was completed on the oxygen contaminated and welded, nitride, carbide, carbonitride, and solid solution strengthened alloys. The effect of the long time aging treatment on the bend ductile brittle transition temperature was determined. Metallographic examination and room temperature hardness traverse data showed a good correlation with the bend test data.

A recommendation for the remaining four-inch diameter ingot scale-up compositions was made to the NASA project manager. A decision from NASA on the next scale-up compositions is expected during the next report period.

Evaluation of the carbide strengthened scale-up composition Ta-8W-1Re-0.7Hf-0.025C (ASTAR-811C) continued. The final annealing temperature was shown to have a significant effect on creep strength and on room temperature tensile properties. Investigation of the relation between the observed property changes and the precipitate morphology and distribution has been initiated. Metallographic examination of the TIG welded tensile specimens which had been tested over the temperature range of -196°C to 1315°C (-320°F to 2400°F) revealed that mechanical twinning had occurred at -196°C (-320°F). At 1315°C (2400°F), the fracture mode was a combination of shear and grain boundary separation.

Chemical analysis data obtained during this quarter shows good agreement between the analyzed oxygen content and the values determined gravimetrically. The results are reported in Table 1 and presented graphically in Figure 1. The weight gain values have been corrected for the residual oxygen content (-20 ppm). The use of weight gain as a reliable technique for in-process control for monitoring oxygen pickup has been described by Lessmann and Stoner⁽²⁾ who have also reported that carbon and nitrogen pickup during the intentional oxygen contamination to be essentially nil. Carbon analysis data for NASV-12 and NASV-20 also reported in Table 1 confirm this earlier observation.

The ductile-brittle bend transition behavior of as-welded and oxygen contaminated and welded specimens that had been heated for 1000 hours at 1800°F (982°C) at pressures below 1×10^{-8} torr was determined. Transition temperature data are recorded in Table 2, along with transition temperature data previously obtained in this study. Included in the 1000 hour run were base metal specimens of NASV-18, 19, and 21, as well as specimens of all six compositions that had been welded, and specimens of all compositions except NASV-19 that had been intentionally oxygen contaminated and welded. Although two levels of oxygen contamination were investigated only those specimens contaminated to nominally 350 ppm O_2 were included in the 1000 hour, 1800°F exposure. As reported previously⁽¹⁾, the specimen of NASV-19 contaminated with 350 ppm O_2 failed during welding and the non-availability of additional oxygen doped material did not permit the inclusion of this composition in the 1000 hour heat treatment.

Generally, the ductile-brittle transition temperature was increased by the 1000 hour, 1800°F exposure. The annealed base metal samples exhibited only a minor increase. However, an increase of as high as $+550^{\circ}\text{F}$ (306°C) was observed for the TIG welded material. The measured decrease in ductility is assumed to be caused by a precipitation reaction or reactions which occurred during the isothermal exposure. In addition to the complexity of the alloys studied, the intentional oxygen contamination, cast weld metal, and the adjacent thermally disturbed

**TABLE 1. Oxygen and Carbon Contamination Data (Weight Gain and Chemical Analyses)
of Intentionally Oxygen-Contaminated Sheet**

Heat No.	Composition	Chemical Analyses (ppm)			
		Oxygen		Carbon	
		Analyzed	Weight Gain	After Oxidation	Prior to Oxidation
NASV-12	Ta-7.5W-1.5Re- 0.5Hf-0.015C- 0.015N	280	285	170	160/190
		370	305		
NASV-13	Ta-6.5W-2.5Re- 0.3Hf-0.01C-0.01N	280	350	--	--
NASV-18	Ta-5W-1Re- 0.3Zr-0.025N	360 (b)	335	--	--
		420	335		
NASV-21	Ta-10W-1Re- 0.5Hf	310 (b)	345	--	--
		310	345		
NASV-20	Ta-8W-1Re- 0.7Hf-0.025C	340	295	212	235
NASV-19	Ta-8.5W-1Re- 1Hf	160	125	--	--

(a) ASTAR-811C

(b) Weld metal

NOTE: Oxygen contamination was accomplished by exposing the specimens to a partial pressure of 500 ppm oxygen in ultra pure helium at temperatures of 800 to 1000°F (427 to 537°C).

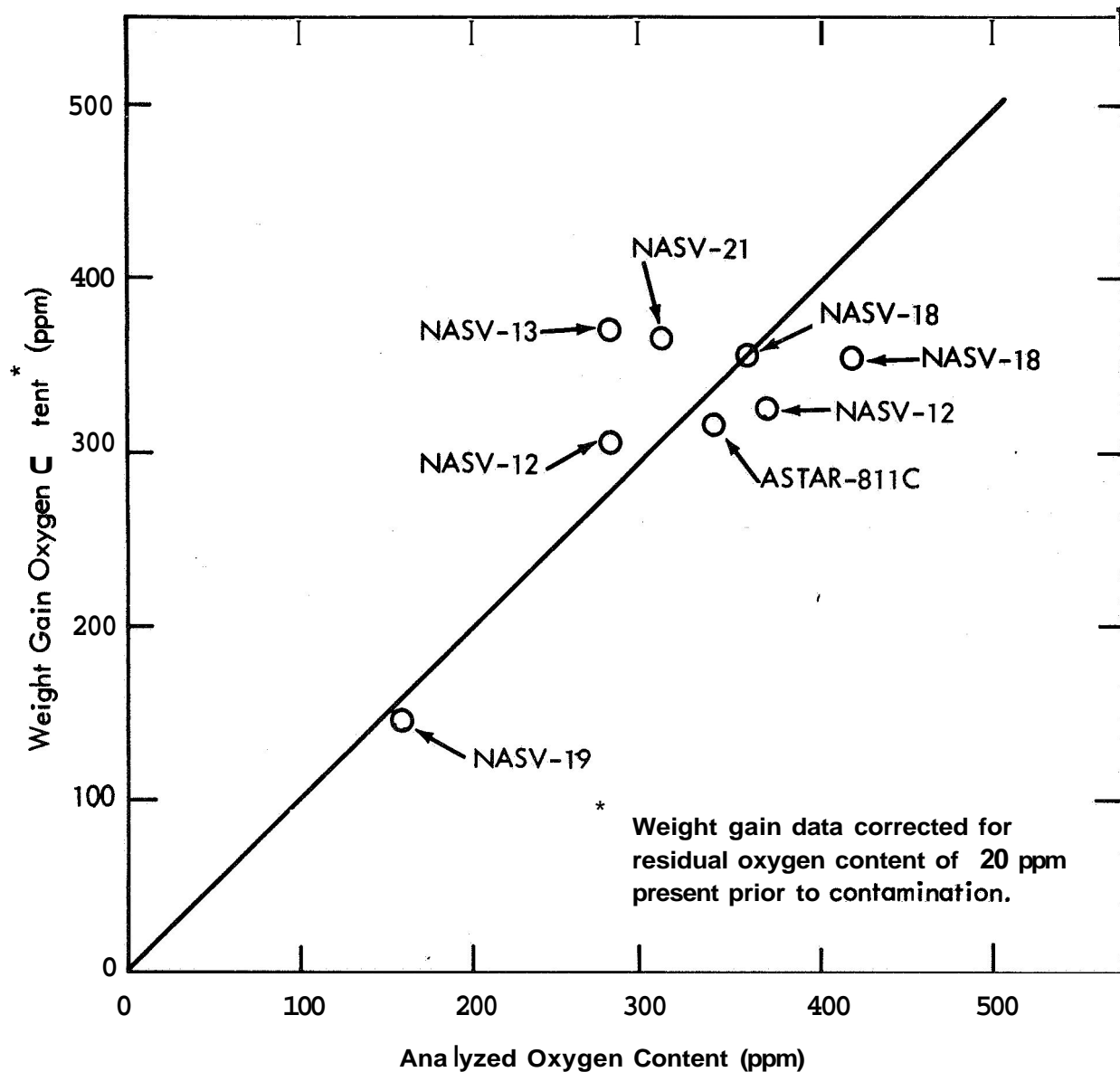


FIGURE 1 - Comparison of Weight Gain Versus Chemical Analyses Determinations of Oxygen Contaminated Tantalum Alloy Samples

TABLE 2. Ductile-Brittle Transition Temperature Results of Weldability and Thermal Stability Study (Compositions NASV-12, 13, 18, 19, 20(a), and 21)

Composition	Ductile-Brittle Transition Temperature (°F)					
	Base Metal	As TIG Welded	Doped(d) and Welded	Base Metal Aged(c)	Welded and Aged(c)	Doped(d) Welded and Aged(c)
Ta-7.5W-1.5Re-0.5Hf-0.015C-0.015N (NASV-12)	-175	+100	+400	--	+200	+600
Ta-6.5W-1.5Re-0.3Hf-0.01C-0.01N (NASV-13)	-225	+100	+450	--	+200	+300
Ta-5W-1Re-0.3Zr-0.02N (NASV-18)	<-320	-250	+400	-300	+300	+800
Ta-8.5W-1.5Re-1.0Hf (NASV-19)	<-320	-250	(b)	<-250	-100	(b)
Ta-8W-1Re-0.7Hf-0.025C (NASV-20)(a)	<-320	-250	+250	--	-100	+200
Ta-10W-1Re-0.5Hf (NASV-21)	<-320	-250	+300	-225	-150	+500

(a) ASTAR-811C (b) All NASV-19 material contaminated with 350 ppm O₂ failed during welding (Ref. 1)
(c) 1000 hours at 1800°F (d) Contaminated with nominally 350 ppm O₂

heat affected zone are factors which compound the difficulty of data interpretation. However, the data in Table 2 indicate that oxygen contamination exerted the greatest effect on the ductile-brittle transition temperature. **Also**, the sensitivity of the **DBTT** to oxygen contamination appeared to be independent of the initial interstitial concentration. For example, the solid solution strengthened alloy (**NASV-21**) contained less than 50 ppm C, O, and N while the **ASTAR-811C (NASV-20)** contains a **250 ppm** carbon addition. However when contaminated with **350 ppm O₂**, the ductile-brittle transition temperature of both are essentially identical.

With a couple of exceptions which will be discussed in more detail later, the loss of ductility was generally accompanied by a decrease in hardness level. Specimens of NASV-21, 20, **18**, and **12** representing the four alloy types:

- (a) Solid Solution
- (b) S. S. + Carbide
- (c) S. S. + Nitride
- (d) S. S. + Carbonitride

were studied metallographically and hardness traverses were taken. It was assumed that during testing, failure of the bend specimens occurred in the area(s) of maximum hardness (i.e., least ductility). That this assumption is valid is shown in Figure 2 where maximum specimen hardness is plotted versus the transition temperature. Fracture within each specimen generally occurred where expected from the hardness data and often did not propagate through the softer area of the specimen corresponding to the minima in the hardness profile.

Hardness traverse data and photomicrographs were taken from transverse weld sections which were:

- a. TIG welded plus 1000 hours at **1800°F**.
- b. Contaminated with 350 ppm O₂ then TIG welded.
- c. (b) plus **1000** hours at **1800°F**.

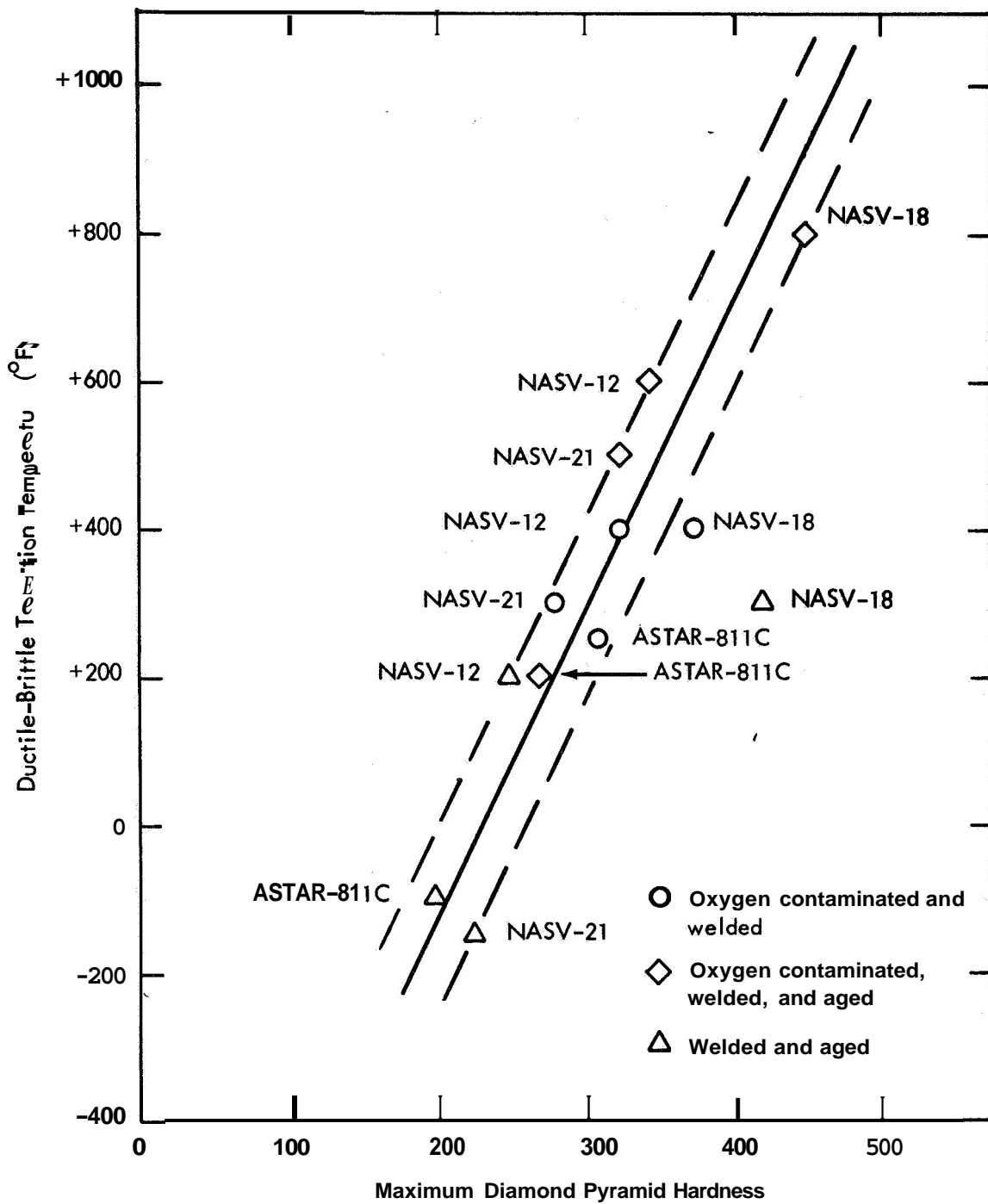


FIGURE 2 - Effect of Maximum Weld Specimen Hardness on Ductile-Brittle Transition Temperature

The hardness traverse data and photomicrographs are presented in Figures 3 through 10. The letter notations on the hardness traverse plots correspond to the area from which the photomicrographs were taken. The local hardness variations measured within the weld metal are probably due to grain orientation and constitutional segregation during freezing. Also the heat affected zone is subjected to a severe thermal disturbance over a broad temperature spectrum. As noted previously these effects coupled with the complexity of the precipitation reaction(s) occurring make quantitative interpretation of the hardness data very difficult. However, a semi-quantitative discussion of the probable precipitation reactions and their effect on low temperature strength of the base metal can be made from the hardness data that were obtained.

The starting sheet material (0.035 inch thick) was annealed for 1 hour at 1650°C (3000°F) prior to oxygen contamination and/or welding. After 1000 hours at 1800°F, the hardness of the matrix has decreased significantly as shown by the data tabulated below.

TABLE 3 - Effect of 1000 Hours at 1800°F on the Hardness of Tantalum Alloy Sheet (Annealed 1 Hour at 1650°C(3000°F) Prior to the Exposure)

Composition	As-Annealed 1 Hr. at 3000°F	Hardness, DPH Plus 1000 Hours at 1800°F	Δ DPH
Ta-10W-1Re-0.5Hf (NASV-22)	230	195	-35
Ta-8W-1Re-7Hf-0.025C (NASV-20)	255	188	-67
Ta-7.5W-1.5Re-0.5Hf-0.015C- 0.015N (NASV-12)	310	228	-82
Ta-5W-1Re-0.3Zr-0.025N (NASV-18)	275	325	+50

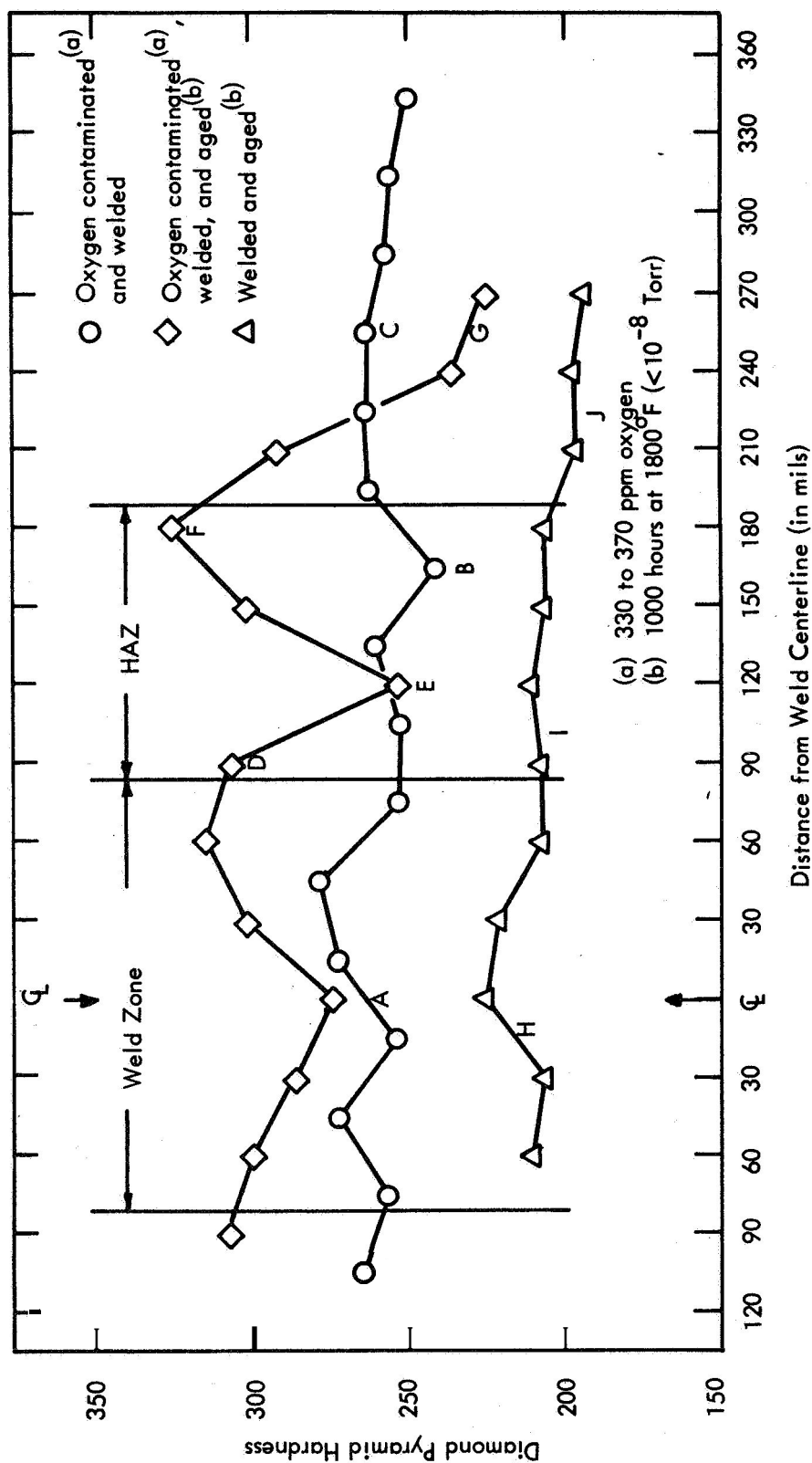
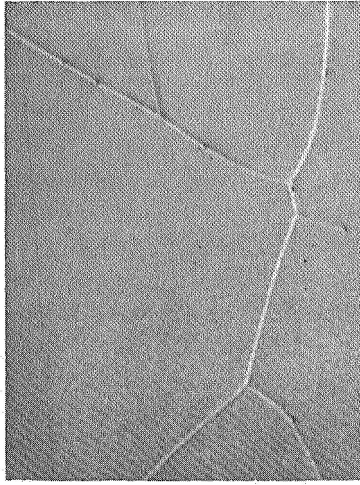
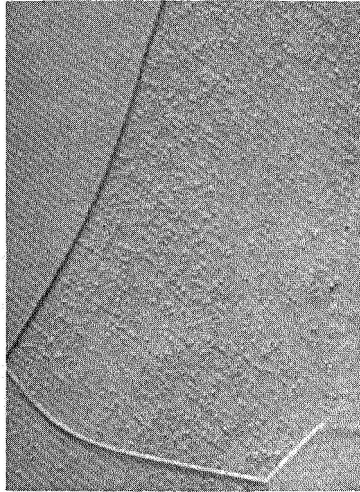


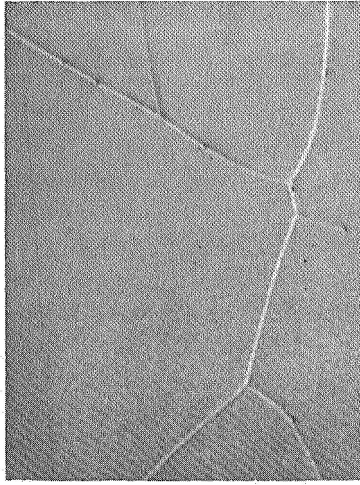
FIGURE 3 - Diamond Pyramid Hardness Transverse of NASV-21 (Ta-10W-1Re-0.5Hf) Weld Specimens



(a) Weld Zone (Point A in Fig. 3)
500X 268 DPH



(b) HAZ (Point B in Fig. 3)
1500X 240 DPH



(c) Base Metal (Point C in Fig. 3)
1500X 263 DPH

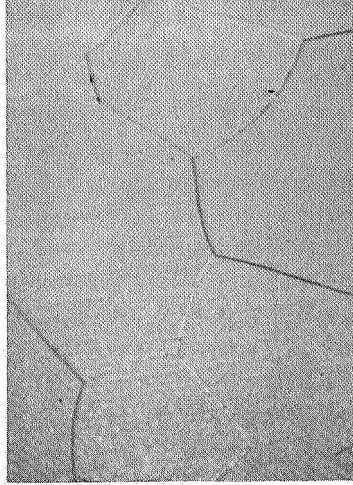
Oxygen Contaminated and Welded Specimen



(d) HAZ (Point D in Fig. 3)
500X 307 DPH



(e) HAZ (Point E in Fig. 3)
1500X 252 DPH

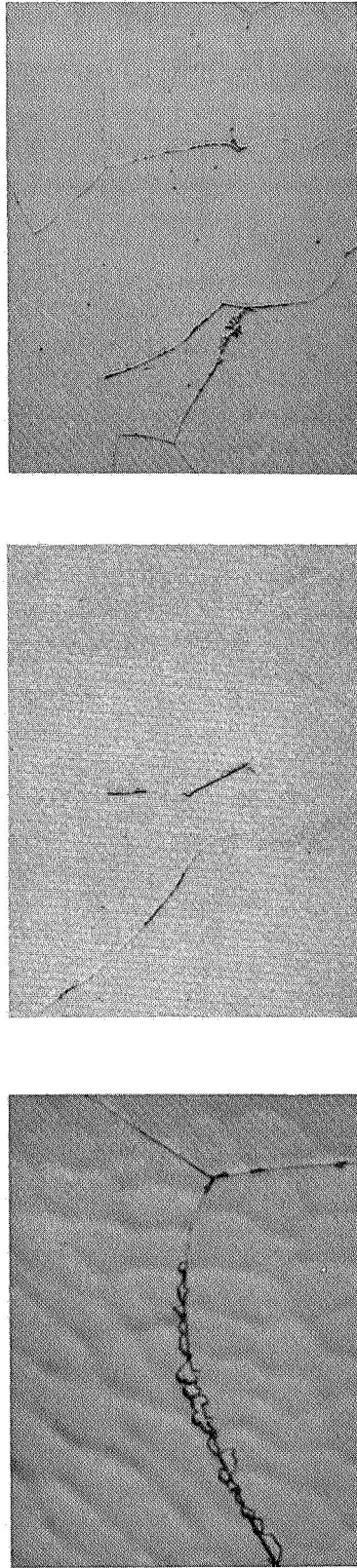


(f) Base Metal (Point G in Fig. 3)
500X 225 DPH

Oxygen Contaminated, Welded, and Aged^(a) Specimen

(a) 1000 Hours at 1800°F ($<10^{-8}$ Torr)

FIGURE 4 - Microstructures of NPSV-21 (Ta-10W-1Re-0.5Hf) Welded Specimens



(g) Weld Zone (Point H in Fig. 3) 1500X 212DPH (h) HAZ (Point I in Fig. 3) 500X 208DPH (i) Base Metal (Point J in Fig. 3) 500X 197DPH

Welded and Aged Specimens

(c) 1000 Hours at 1800°F ($<10^{-8}$ Torr)

FIGURE 4 (Continued) – Microstructure of NASV-2H (T₀-10W-1R₀-0.5Hf) Welded Specimens

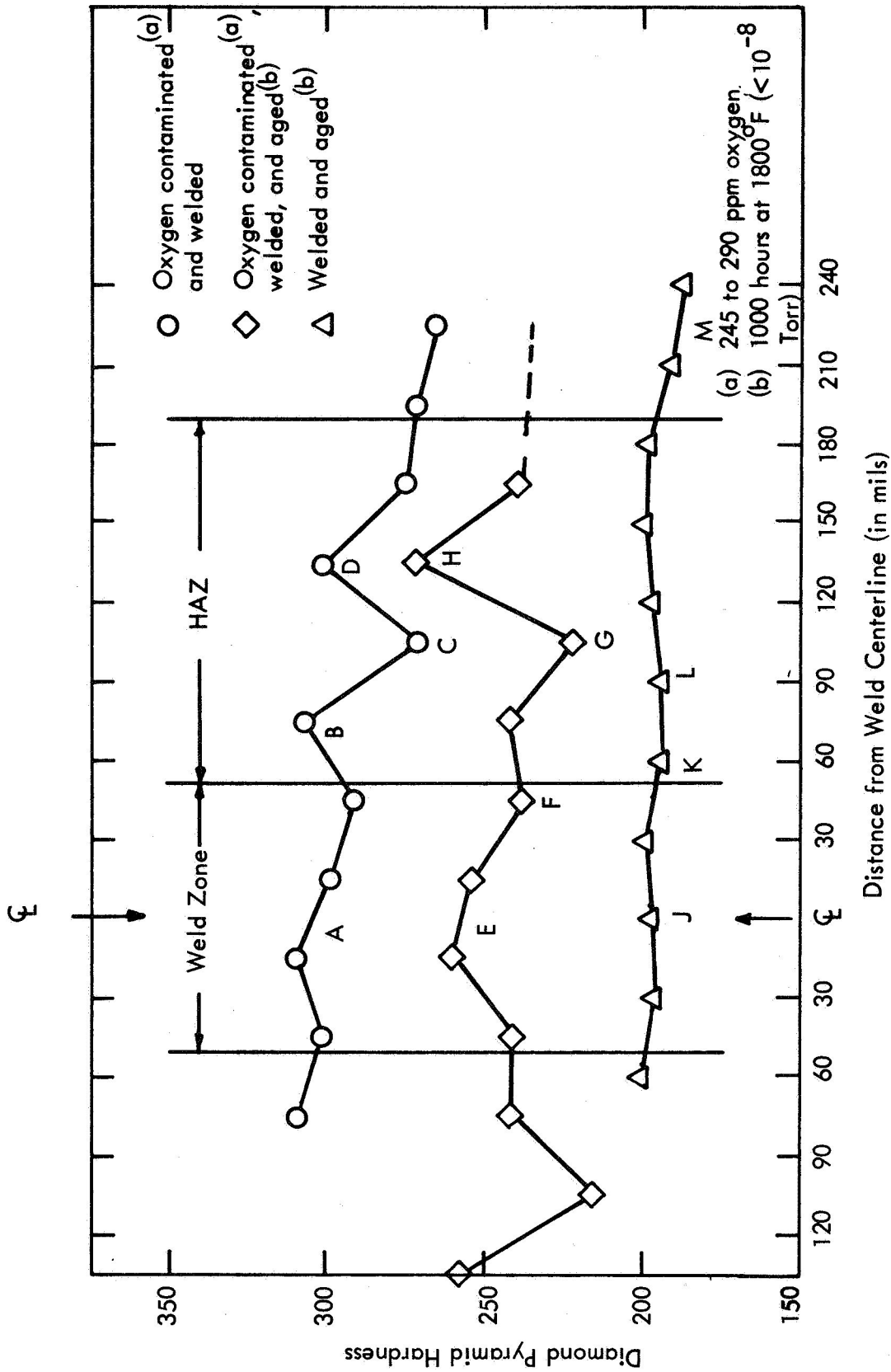
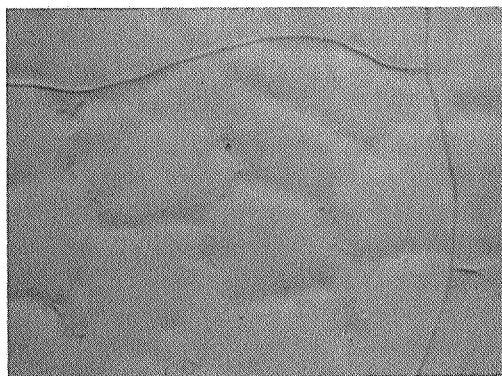
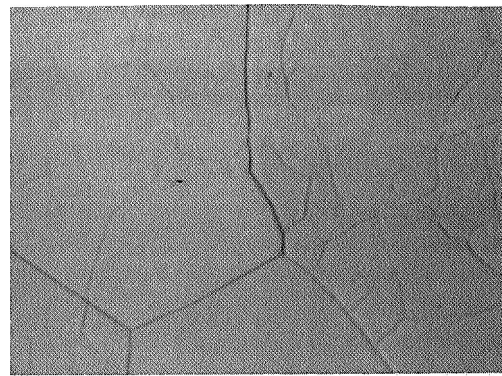


FIGURE 5 - Diamond Pyramid Hardness Traverses of ASTAR-811C (Ta-8W-1Re-0.7Hf-0.025C) Weld Specimens

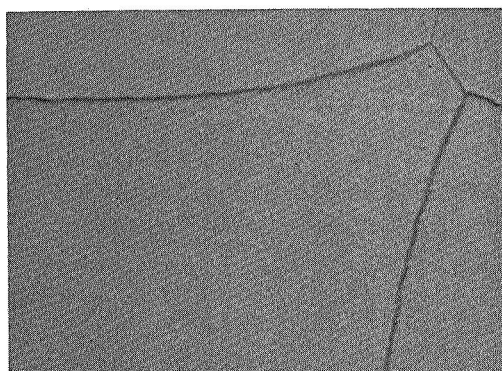


(a) Weld Zone (Point A in Fig. 5) 1500X
305 DPH

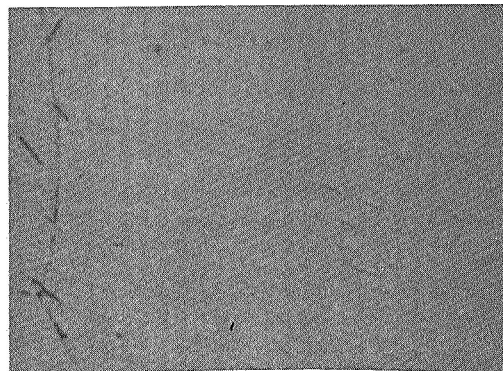


(b) HAZ (Point B in Fig. 5) 1500X
305 DPH

Oxygen Contaminated and Welded Specimen

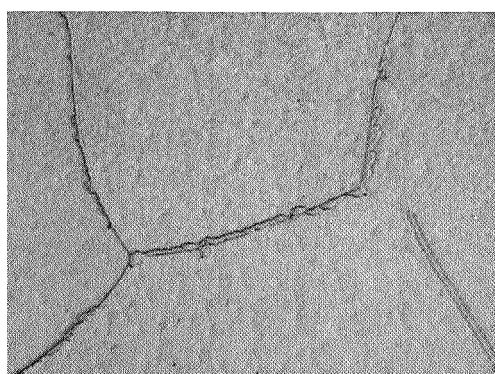


(c) HAZ (Point C in Fig. 5) 1500X
270 DPH

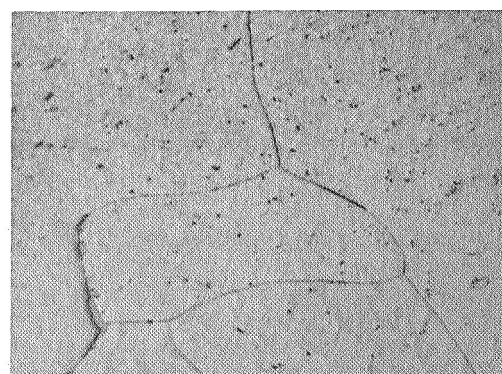


(d) HAZ (Point D in Fig. 5) 1500X
300 DPH

Oxygen Contaminated and Welded Specimen



(e) Weld Zone (Point E in Fig. 5) 500X
255 DPH

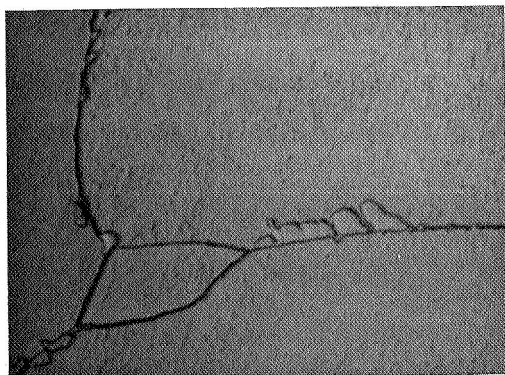


(f) Weld Zone (Point F in Fig. 5) 500X
262 DPH

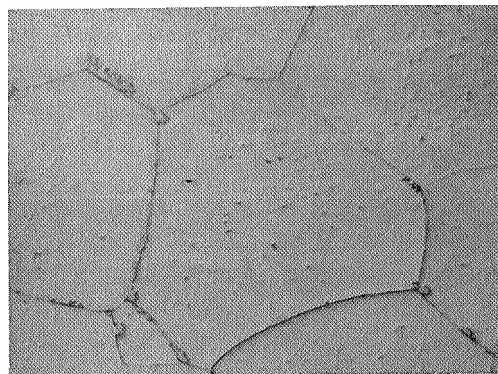
Oxygen Contaminated, Welded, and Aged Specimen

(a) 1000 Hours at 1800°F ($<10^{-8}$ Torr)

FIGURE 6 - Microstructures of ASTAR-811C(Ta-8W-1Re-0.7Hf-0.025C) Welded Specimens

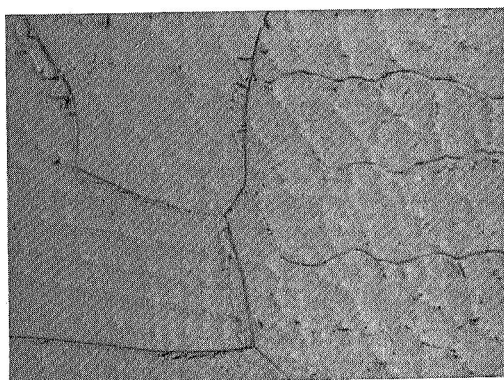


(g) HAZ (Point G in Fig. 5) 1500X
223 DPH

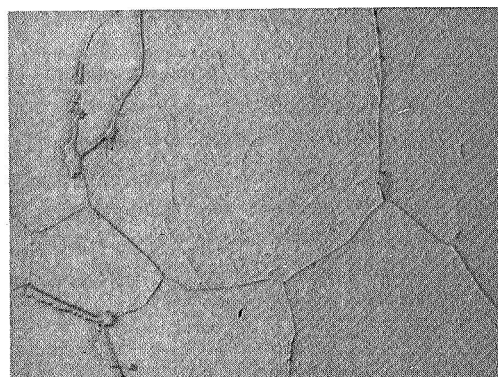


(h) Base Metal (Point I in Fig. 5) 500X
220 DPH

Oxygen Contaminated, Welded, and Aged^(a) Specimen

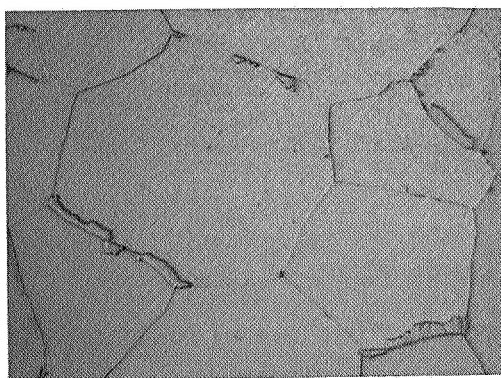


(i) Weld Zone (Point J in Fig. 5) 500X
195 DPH

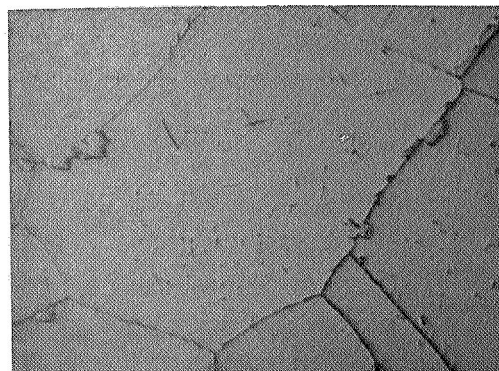


(j) HAZ (Point K in Fig. 5) 500X
190 DPH

Welded and Aged^(a) Specimen



(k) HAZ (Point L in Fig. 5) 500X
190 DPH



(e) Base Metal (Point M in Fig. 5) 500X
188 DPH

Welded and Aged^(a) Specimen

(a) 1000 Hours at 1800°F ($<10^{-8}$ Torr)

FIGURE 6 (Continued) - Microstructures of ASTAR 811-C (Ta-8W-1Re-0.7Hf-0.025C)
Welded Specimens

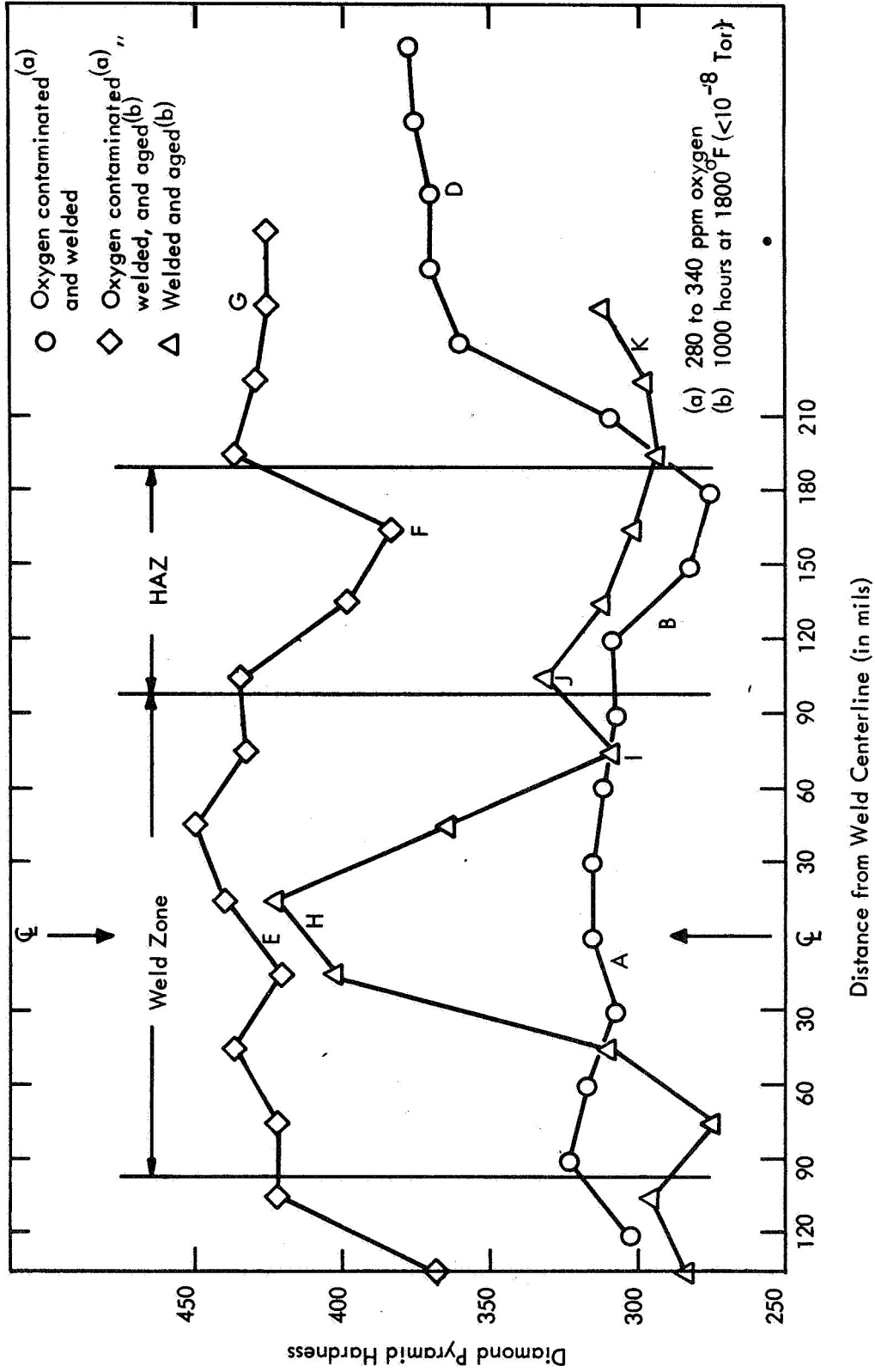
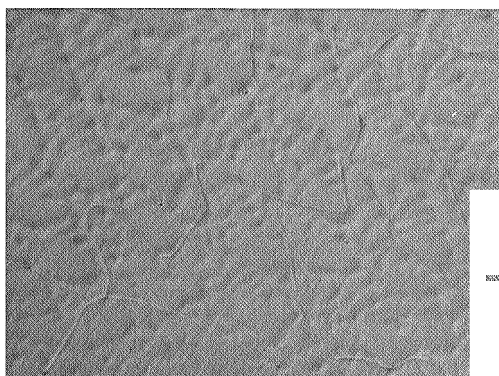
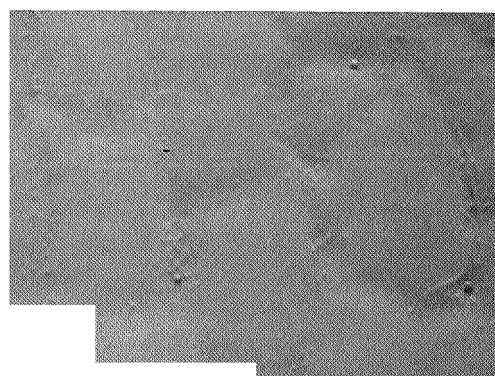


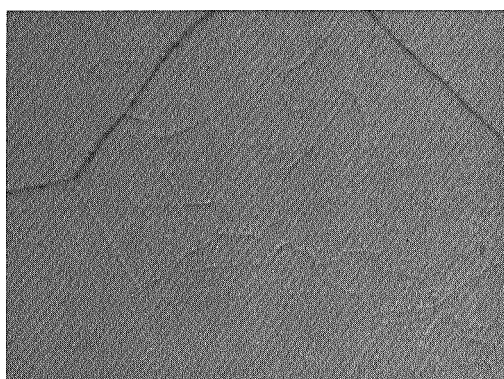
FIGURE 7 - Diamond Pyramid Hardness Traverses of NASV-18 (Ta-5W-1Re-0.3Zr-0.025N) Weld Specimens



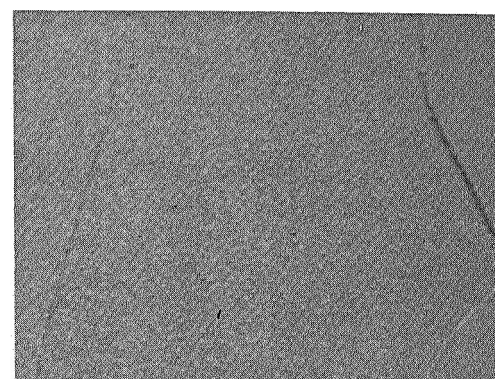
(a) Weld Zone (Point A in Fig. 7) 500X
315 DPH



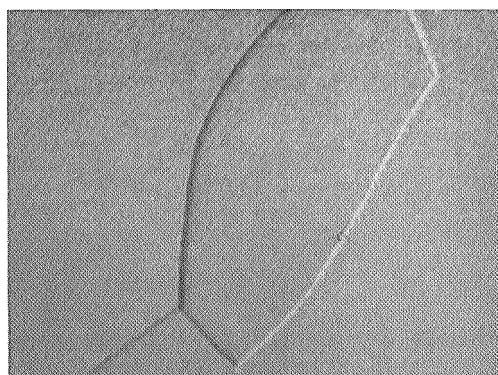
(b) Weld Zone (Point A in Fig. 7) 1500X
315 DPH



(c) HAZ (Point B in Fig.7) 1500X
300 DPH



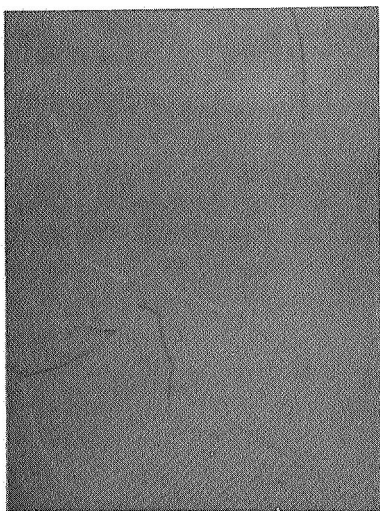
(d) HAZ (Point C in Fig. 7) 1500X
275 DPH



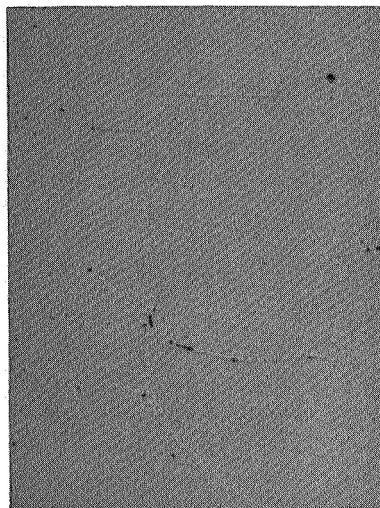
(e) Base Metal (Point D) in Fig.7) 1500X
370 DPH

Oxygen Contaminated and Welded Specimens

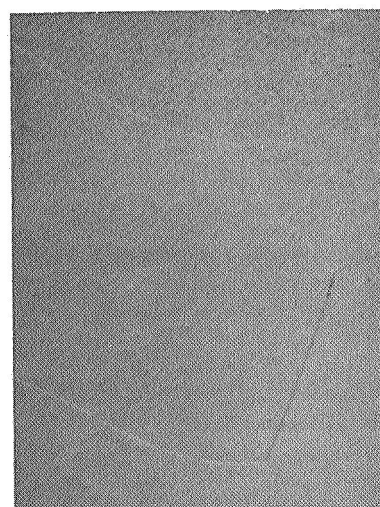
FIGURE 8 - Microstructures of NASV-18 (Ta-5W-1Re-0.3Zr-0.02N) Welded Specimens



(f) Weld Zone (Point E in Fig. 7)
500X 430 DPH



(f) HAZ (Point F in Fig. 7)
500X 383 DPH

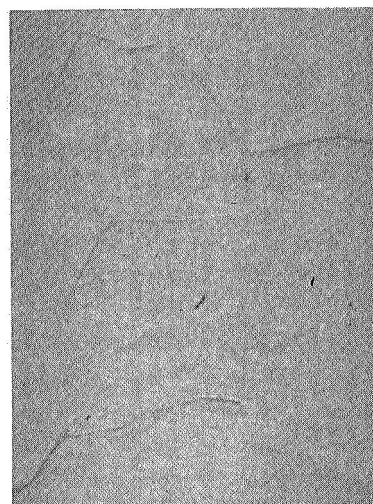


(h) Base Metal (Point G in Fig. 7)
500X 425 DPH

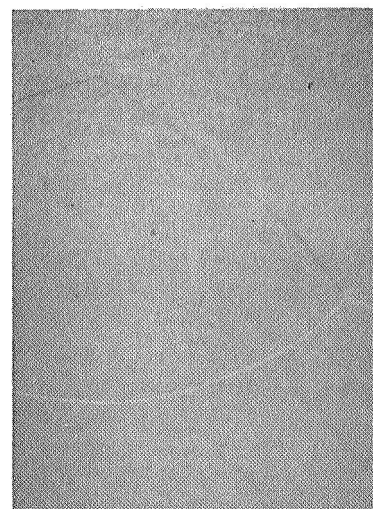
Oxygen Contaminated, Welded and Aged^(a) Specimen



(k) Base Metal (Point K in Fig. 7)
1500X 305 DPH



(i) H0Z (Point J in Fig. 7)
500X 332 DPH



(i) Weld Zone (Point H in Fig. 7)
500X 308 DPH

Welded and Aged^(a) Specimen

(a) 1000 Hours at 1800°F ($<10^{-8}$ Torr)

FIGURE 8 (Continued) - Microstructures of NASV-18 (Ta-5W-1Re-0.3Zr-0.02N) Welded Specimens

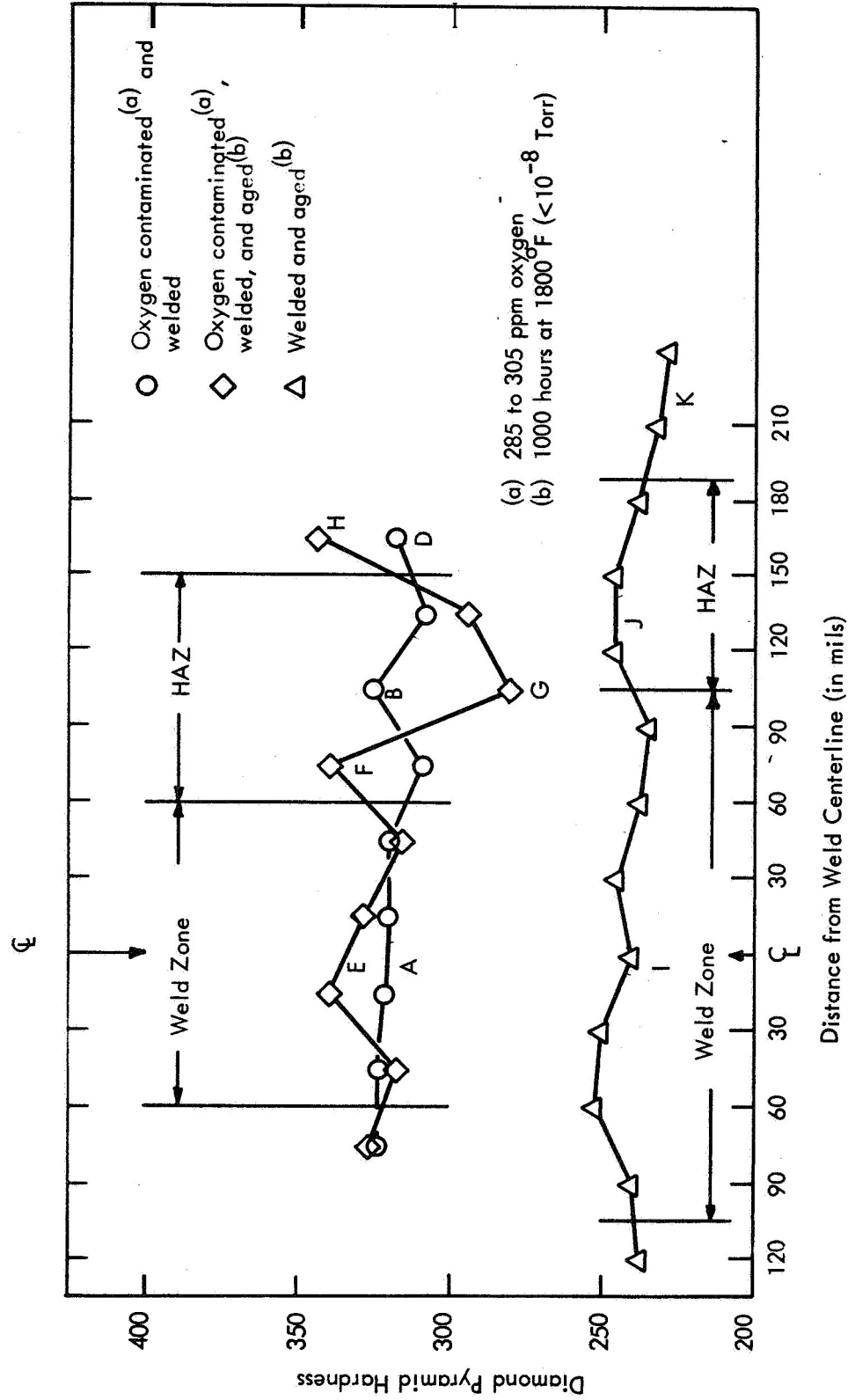
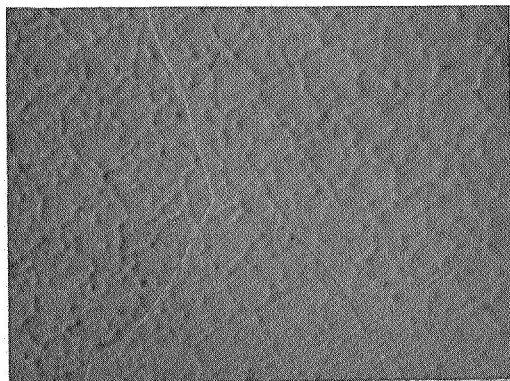
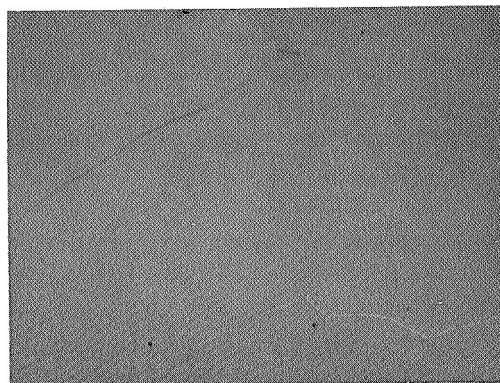


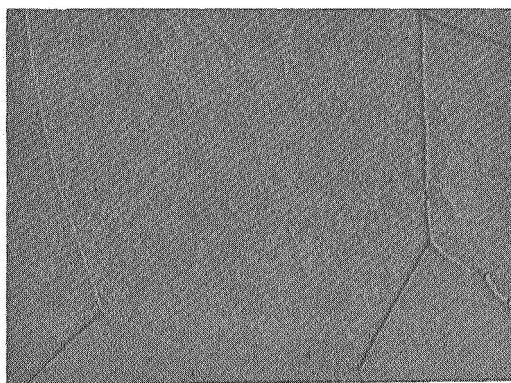
FIGURE 9 - Diamond Pyramid Hardness Traverses of NASV-12 (Ta-7.5W-1.5Re-0.5Hf-0.015C-0.015N) Weld Specimens



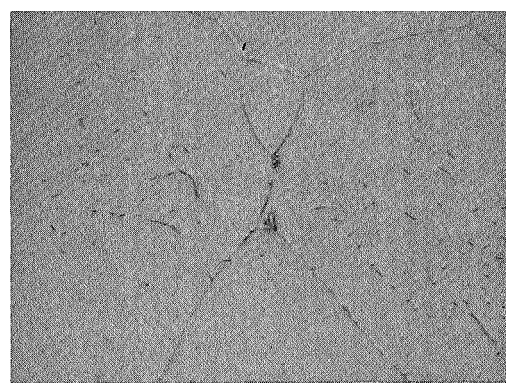
(a) Weld Zone (Point A in Fig. 9) 500X
320 DPH



(b) HAZ (Point B in Fig. 9) 500X
325 DPH



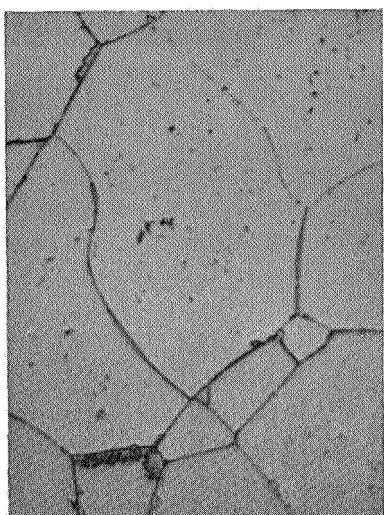
(c) HAZ (Point C in Fig. 9) 1500X
308 DPH



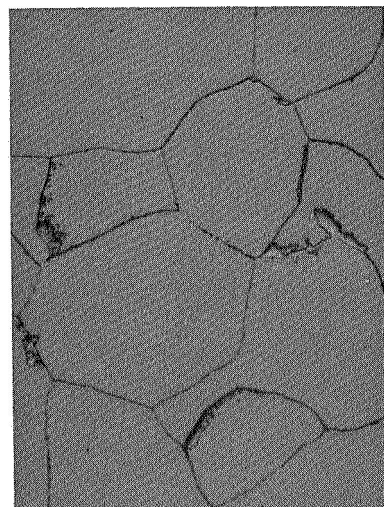
(d) Base Metal (Point D in Fig. 9) 500X
318 DPH

Oxygen Contaminated and Welded Specimen

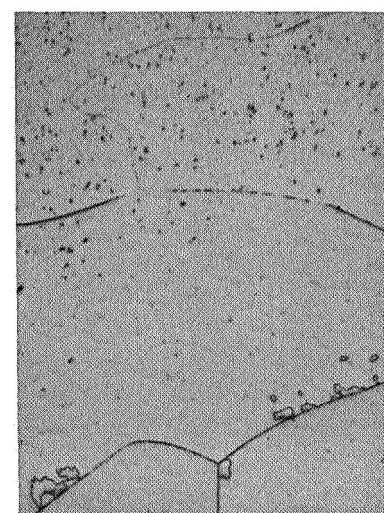
FIGURE 10 - Microstructures of NASV-12 (Ta-7.5W-1.5Re-0.5Hf-0.015C-0.015N)
Welded Specimens



(e) Weld Zone (Point L in Fig. 9)
500X 335 DPH



(f) HAZ (Point F in Fig. 9)
500X 340 DPH

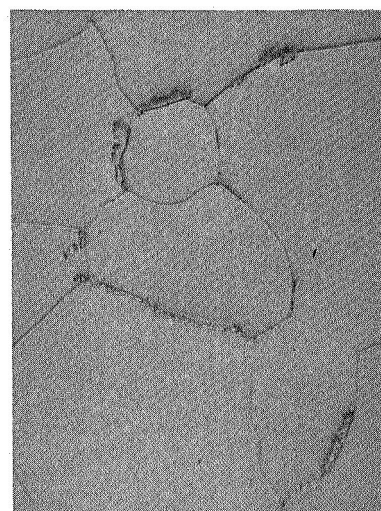


(g) Base Metal (Point H in Fig. 9)
500X 345 DPH

Oxygen Contaminated, Welded, and Aged (a) Specimen



(h) Weld Zone (Point I in Fig. 9)
500X 240 DPH



(i) HAZ (Point J in Fig. 9)
500X 245 DPH



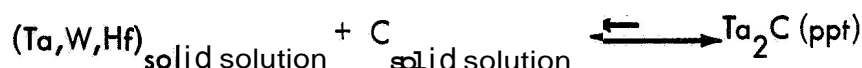
(j) Base Metal (Point K in Fig. 9)
500X 230 DPH

Welded and Aged (a) Specimen

(a) 1000 Hours at 1800°F (10^{-8} Torr)

FIGURE 10 (Continued) - Microstructures of NASV-12 (Ta-1.5Re-0.5Hf-0.015C-0.015N) Welded Specimens

During the final annealing treatment at 3000°F all or part of the carbon and/or nitrogen addition was taken into solution. Previous work⁽²⁾ in this investigation, has shown that carbon precipitates from solid solution, from a Ta-W matrix containing ≤ 1 at% reactive metal (Hf, Zr) additions, during exposure at temperatures as low as 700°C by the following reaction.



The hardness of the matrix has always been lowered by this reaction indicating that the dimetal carbide forms a discrete non-coherent second phase particle. The decrease in hardness observed for the solid solution composition Ta-10W-1Re-0.5Hf (NASV-21) is attributed to precipitation of the residual carbon (-32 ppm) as Ta_2C . This data would indicate that the carbon solubility in the matrix is certainly low at 1800°F. The nitride strengthened composition Ta-5W-1Re-0.3Zr-0.025N (NASV-18) showed a 50 DPH increase in hardness as a result of the 1000 hour exposure at 1800°F. The hardness increase is attributed to coherent precipitation reaction. Previous work has shown that the nitride precipitation in a tantalum alloy matrix may follow classical age hardening behavior^(20,21) by the following reaction.



The kinetics of this reaction and the degree of strengthening of course are dependent on the aging temperature, aging time, and degree of supersaturation.

Thus in the carbonitride containing composition (NASV-12) both reactions are occurring simultaneously. However, the hardness data in Table 3 would indicate that the carbide precipitation reaction predominated during the 1800°F exposure.

Oxygen was added to the base metal by formation of an adherent oxide film at approximately 1100°F which was then subsequently diffused in by annealing for 50 hours at 1800°F. The detailed experimental procedure is described elsewhere⁽²²⁾. Introducing oxygen to the matrix in this manner results in an increase in the room temperature hardness. (See Table 4). Work by Rowcliffe, et al⁽³⁾ showed that a coherent oxide precipitate was formed when Cb-1Zr or Cb-1W-1Zr sheet was exposed to a low oxygen partial pressure at 800-1000°C. The observed

TABLE 4 - Hardness of Oxygen Contaminated Initial Alloys Before and After Exposing for 1000 Hours at 1800°F

Heat No.	Initial ^(a) Condition DPH	Oxygen Contaminated					$\partial \rho \text{DPH} / \partial C^{(d)}$
		Oxygen Level		$A_s^{(b)}$ Contaminated DPH	$\partial \Delta D \text{ P} / \partial C^{(c)}$	O_2 Contaminated Plus 1000 Hrs. at 1800°F DPH	
		Weight %	Atom %				
NASV-21	230	0.021	0.24	255	104	225	125
NASV-20	255	0.0295	0.33	265	30	235	143
NASV-12	310	0.029	0.33	318	24	340	340
NASV-18	275	0.0335	0.38	375	263	425	263

(a) Annealed 1 Hour at 1650°C (3000°F)

(b) Doped at 1100°F and then diffusion annealed 50 Hours at 1800°F.

(c) $\Delta DPH/\Delta C$, change in hardness per atom percent oxygen added, $\Delta DPH = DPH_{as\ doped} - DPH_{as\ annealed}$

(d) $\Delta DPH = DPH_{contaminated\ 1000\ Hrs\ at\ 1800^\circ F} - DPH_{annealed\ 1000\ Hrs\ at\ 1800^\circ F}$

increase in both the low temperature and elevated temperature properties was attributed to a coherent ZrO_2 precipitate⁽³⁾.

2

The strengthening of the tantalum alloy matrix by the oxygen contamination is assumed to be caused by a similar reaction. The strengthening effect of the oxygen addition was evaluated using room temperature hardness values. The change in hardness per atom percent oxygen ($\partial \Delta DPH / \partial C$) added was then calculated and the values obtained are listed in Table 4. For material in the as-contaminated condition, values of $\partial \Delta DPH / \partial C$ of 24-30 were observed for the carbide and carbonitride strengthened compositions and 100-250 for the solid solution and nitride strengthened composition. The values of 24-30 for $\partial \Delta DPH / \partial C$ appear low. Adding oxygen to columbium and tantalum result in values for $\partial \Delta DPH / \partial C$ of 140 and 170 respectively⁽²⁴⁾ and are representative values for interstitial hardening in BCC metals⁽²³⁾. This is in contrast to values of $\partial \Delta DPH / \partial C$ of 10-20 for substitutional solute strengthening additions (i.e., W, Re, Hf, Mo)^(23,24). As contaminated (See Figure 4a), the microstructure is single phase when examined at 1500X, and as previously noted, it is assumed that the oxygen combines with the reactive metal (Hf) to form a coherent HfO_2 precipitate. The strengthening of the coherent precipitate ($\partial \Delta DPH / \partial C$) will be on the same order of magnitude as that observed for the interstitial solid solution strengthening. After exposing for 1000 hours at 1800°F, the $\partial \Delta DPH / \partial C$ values for the strengthening contribution of the oxygen addition are consistent. The low values of $\partial \Delta DPH / \partial C$ for NASV-12 and 20 in the as-contaminated condition most probably resulted from carbide precipitation during the 50 hour homogenizing treatment. The values of $\partial \Delta DPH / \partial C$ for NASV-12 (carbonitride) and NASV-18 (nitride) after the 1000 hour exposure are 2 to 3 times that for the solid solution (NASV-21) and carbide strengthened (NASV-20) composition and no doubt reflects the additive contribution of the nitride precipitation reaction.

The strengthening effects of the oxygen, nitrogen, and carbon on the tantalum alloy matrix are very complex. The interesting strength properties resulting from the various precipitation reactions will require much more investigation before they are understood, particularly their effect on elevated temperature strength.

B SCALE-UP INVESTIGATION

Evaluation of the 18 inch wide x 33 inch x 0.04 inch thick sheet of ASTAR-811C (Heat No. NASV-20WS) was made. Chemical analysis, mechanical properties and weldability characteristics were determined and were similar to those obtained previously on material processed by the standard procedure⁽⁴⁾. The processing of NASV-20WS which was described in the 8th Quarterly Progress Report varied significantly from the standard processing schedule. NASV-20WS was processed from a section of side forged ingot which has been annealed* for 2 hours at 1480°C (2700°F) and then rolled from a thickness of 1-1/8 inch to 1/4 inch at 500°C (930°F). After conditioning, the 0.24 inch plate was annealed for 1 hour at 1480°C (2700°F) and rolled at room temperature to a 0.04 inch sheet, a final total reduction of 83%. The standard processing schedule would have been to anneal the 0.24 inch plate at 1650°C (3000°F), roll to 0.06 inch, anneal at 1700°C (3090°F), and then roll to 0.04 inch, the final reduction being 33%.

Chemical analysis results on this sheet were 200 ppm carbon, 20 ppm nitrogen, and 13 ppm oxygen. These values are in excellent agreement with those previously obtained on the NASV-20 (ASTAR-811C) as-cast ingot (230 to 240 ppm carbon, 13 to 27 ppm oxygen). The bend ductile-brittle transition temperature of the as-TIG welded NASV-20WS sheet was less than -100°C (-150°F) and compares with the transition temperature for as-TIG welded sheet material processed by the standard schedule from both the side forged and the upset forged billets (Table 5). The 1 hour recrystallization behavior, including microstructure, hardness, and grain size data, on the large sheet is recorded in Table 6. Similar data previously obtained on 0.04-inch and 0.06-inch sheet that had been reduced 33 and 73% respectively are also recorded in Table 6.

A comparison of the tensile data with that previously obtained is given in Table 7. All specimens were annealed for 1 hour at 1650°C (3000°F) prior to testing. Excellent agreement exists between the two sets of data at -195°C (-320°F) and at room temperature. The strength at

*Annealing done at $< 5 \times 10^{-5}$ torr.

TABLE 5. Ductile-Brittle Transition Temperature of ASTAR-811C^(a) (Ta-8W-1Re-0.7Hf-0.025C) in As-TIG Welded Condition

Material	Temperature		No Load Bend Angle (Degrees)	Remarks	DBTT	
	°F	°C			°F	°C
18" by 33" ^(b) Sheet (NASV-20WS)	-150	-101	95	Bend	<-150	<-101
	-250	-157	92	Slight brittle failure, weld metal		
	-250	-157	93	Brittle failure, weld metal		
Sheet from ^(b) side forging	-150	-101	95	Bend	<-150	<-101
	-200	-129	60	Slight ductile failure, weld metal		
Sheet from ^(c) upset forging	-250	-157	95	Bend	<-250	<-157

(a) Heat NASV-20

(b) 0.040 inch sheet reduced 83% then annealed for 1 hour at 1650°C/3000°F prior to welding.
Bend radius of 1.8t used.

(c) 0.035 inch sheet reduced 33% then annealed for 1 hour at 1650°C/3000°F prior to welding.
Bend radius of 1.0t used.

TABLE 6. Room Temperature Hardness, ^(a) Microstructure, ^(b) and Grain Size ^(c) of As-Rolled ASTAR-811C (NASV-20) (Ta-8W-1Re-0.7Hf-0.025C) Sheet ^(d) After Annealing for 1 Hour at Temperature

Thickness	Prior Reduction (%)	One Hour Annealing										
		Temperature (°C/°F)										
		As-Rolled	1200 2190	1300 2370	1400 2550	1500 2730	1600 2910	1700 3090	1800 3270	1900 3450	2000 3630	
0.04" Sheet	33.3	321 W	282 W	283 W	263 R _B	258 R _X	254 R _X	245 R _X	240 R _X	248 R _X	246 R _X	
		--	--	--	--	0.020	0.023	0.043	0.063	0.091	0.182	
0.06" Sheet	72.5	387 W	319 W	252 R ₉₀	245 R _X	263 R _X	260 R _X	253 R _X	253 R _X	250 R _X	248 R _X	
		--	--	--	0.011	0.013	0.017	0.033	0.057	0.091	0.167	
0.04" Sheet (NASV-20WS)	0	350 W	313 R _B	249 R ₅₀	232 R _X	258 R _X	251 R _X	257 R _X	242 R _X	242 R _X	248 R _X	
		--	--	--	--	0.009	0.013	0.025	0.048	0.120	0.200	

(a) DPH, 30 Kg Load

(b) Microstructure

W - Wrought

R_B - Recrystallization just beginning

R₅₀ - About 50% recrystallized

R₉₀ - About 90% recrystallized

R_X - Fully recrystallized

(c) Grain size in mm, as determined by standard line intercept method.

(d) Sheet processed from side forged 4 inch diameter ingot.

TABLE 7. Mechanical Properties^(a) of ASTAR-811C (Heat NASV-20)

Test Temperature (°F)	Remarks	0.2% Yield Strength (psi)	Ultimate Tensile Strength (psi)	% Elongation		% Reduction in Area
				Uniform	Total	
RQ	b	882,40	105,400	16.2	24.8	51.9
RQ	c	885,00	105,400	16.9	25.9	49.9
-320	b	1 4,000	166,500	19.3	25.1	41.0
-320	c	147,700	165,300	22.0	26.3	41.9
2200	b	29,600	44,500	--	32.5	--
2200	c	3 1600	49,000	--	28.8	--
2400	b	27,400	38,300	--	37.8	--
2400	c	30,400	40,900	--	35.0	--

(a) Specimen annealed for 1 hour at 1650°C (3000°F) prior to test

(b) NASV-20WS (83% reduction prior to final anneal).

(c) Processed by standard schedule. (33% reduction prior to final anneal)

1204 and 1316°C (2200 and 2400°F) for the NASV-20WS sheet material is approximately 10% less than for material processed by the standard schedule. This difference in strength may be explained by the difference in the annealed grain size (i.e., 0.033 mm for the standard processed material versus 0.017 mm for the NASV-20WS sheet).

1. Mechanical Properties

a. Creep Properties. Evaluation of the creep behavior of ASTAR-811C continued this period. Investigated were the effect of final annealing temperature and TIG welding on creep behavior. The data obtained is in Table 8.

Increasing the final annealing temperature from 1650°C to 2000°C (3000 to 3630°F) resulted in a significant increase in the creep resistance of ASTAR-811C at 2400°F and 15,000 psi (Table 8). Correspondingly, the grain size increased from 0.033 mm to 0.2 mm. The increase in creep resistance can be plotted as a linear function of the square root of the grain diameter (Figure 11). The creep rate plotted in Figure 11 is the reciprocal of the time to reach 1% elongation, a parameter which has been used to evaluate creep resistance because of the unique shape of the creep curves⁽⁴⁾. However, the creep curve for the specimen annealed at 2000°C (3630°F) prior to test exhibited essentially a linear curve to over 1% strain.

The mechanism which resulted in the functional relationship shown in Figure 11 is not readily apparent. The effect of grain size on creep behavior has been reported on a number of FCC metals and alloys (5-10). Feltham and Meakin⁽⁹⁾ have shown for copper at 500°C ($0.6T_m$) that the creep rate is proportional to the square of the diameter, with the creep rate increasing with increasing grain diameter. Lead at 25°C ($0.5T_m$) however, exhibits a decrease in creep rate with increasing grain size⁽¹⁰⁾. One of the most significant observations reported however, is that there is apparently an optimum grain size for optimum creep resistance^(5,6,7,8). This observation was made by Hanson⁽⁵⁾ as early as 1939. Crussard⁽⁶⁾ showed a minima in the secondary creep rate as a function of grain size for zinc tested at 95°C ($0.55T_m$) and aluminum tested at 200°C ($0.5T_m$). His explanation was based on transition of the major

TABLE 8. Creep Results on ASTAR-811C

Specimen	Condition	Test Temp (°F)	Stress (psi)	Test Time (hrs)	Total Elongation (%)	Time to 1% Strain	R.T. Hardness, DPH	
							Pre-test	Post-test
NASV-20B-3C	Annealed 1 hr at 1650°C (3000°F) prior to test	2400	15,000	555	2.53	262	249	229
NASV-20-18-100	Annealed 1 hr at 1800°C (3270°F) prior to test	2400	15,000	507	2.00	290	249	226
NASV-20-20-10	Annealed 1 hr at 2000°C (3630°F) prior to test	2400	15,000	1003	2.10	474	260	231
NABV-20-3F-TIGW-1	TIG weld, tested in longitudinal direction (a)	2400	15,000	670	6.03	171	265	227
NABV-20-TIGW-2	TIG weld, tested in longitudinal direction (a)	2000	10,000	194	4.20	69.5	263	232

(a) Tested in As-TIG welded condition.

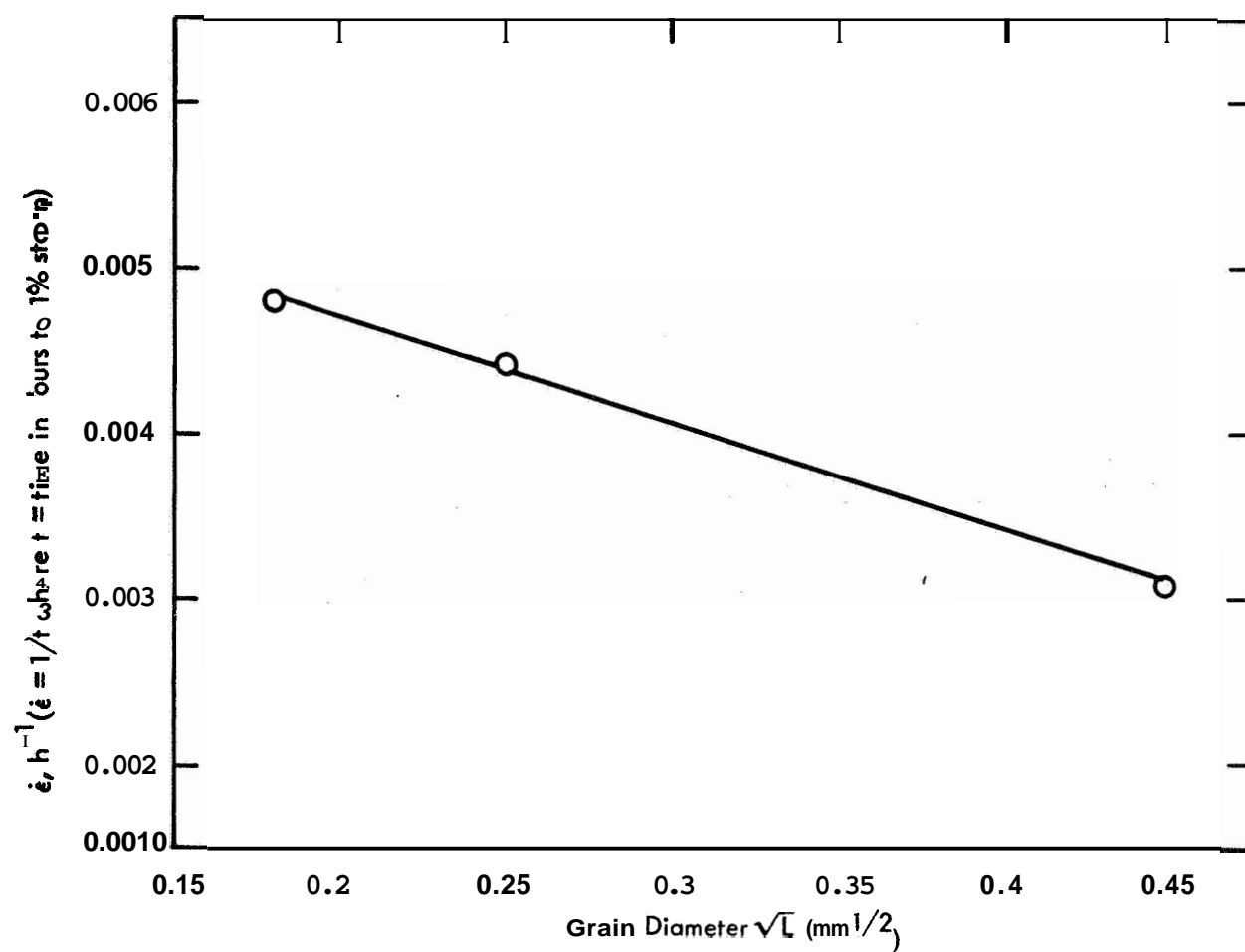


**FIGURE 11 - Effect of Grain Size on Creep Rate of ASTAR-811C
at 2400°F**

deformation process from the boundary to the grain as the volume-to-boundary ratio increased with each process of equal importance at the optimum grain size. Shahinian and Lone⁽⁷⁾ in their study of monel related the observed behavior to the equi-cohesive temperature (T_E)*. At low temperature ($<T_E$) increasing grain size caused reduced rupture life and increased the creep rate while at high temperature ($>T_E$) there was an optimum size for maximum rupture time which varied with test temperature and applied stress. Garafalo⁽⁸⁾ also demonstrated similar high temperature behavior for an austenitic stainless steel. However, data reported has generally been for FCC solid solution strengthened metals and a paucity of data are available for BCC refractory metals. Begley and Cornie⁽¹¹⁾ have shown completely opposite behavior for a solid solution columbium base alloy and a carbide strengthened columbium base alloy. Increasing grain size resulted in increased creep rate for the solid solution alloy while the creep rate of the carbide strengthened alloy decreased.

In addition to the increase in grain size, preliminary examination of the extracted dispersed phase from the creep specimen has revealed a change in the carbide morphology as the annealing temperature was increased. Thus it is not possible at this time to separate the effects of grain size and precipitate morphology. More detailed examination of the creep specimens are in progress. However it will be necessary to perform a similar experiment on a solid solution tantalum base alloy to determine the individual contributions of the grain size and dispersed phase on the creep behavior.

As-TIG welded ASTAR-811C tested with the weld bead parallel to the gauge length showed a significant decrease in creep resistance at 2400°F and 15,000 psi (Table 8). Base metal data are not available at 2600°F so no comparison can be made directly. However the data plotted in Figure 12, on a Larson-Miller plot, indicate that the TIG welds have lower creep resistance than the base metal. The decrease in creep resistance of the TIG welded material may be due to a combination of unfavorable grain orientation of the large as-cast grains and compositional heterogeneity in the fusion zone. The detailed study of the

*The temperature at which the failure mode changes from intragranular to intergranular,

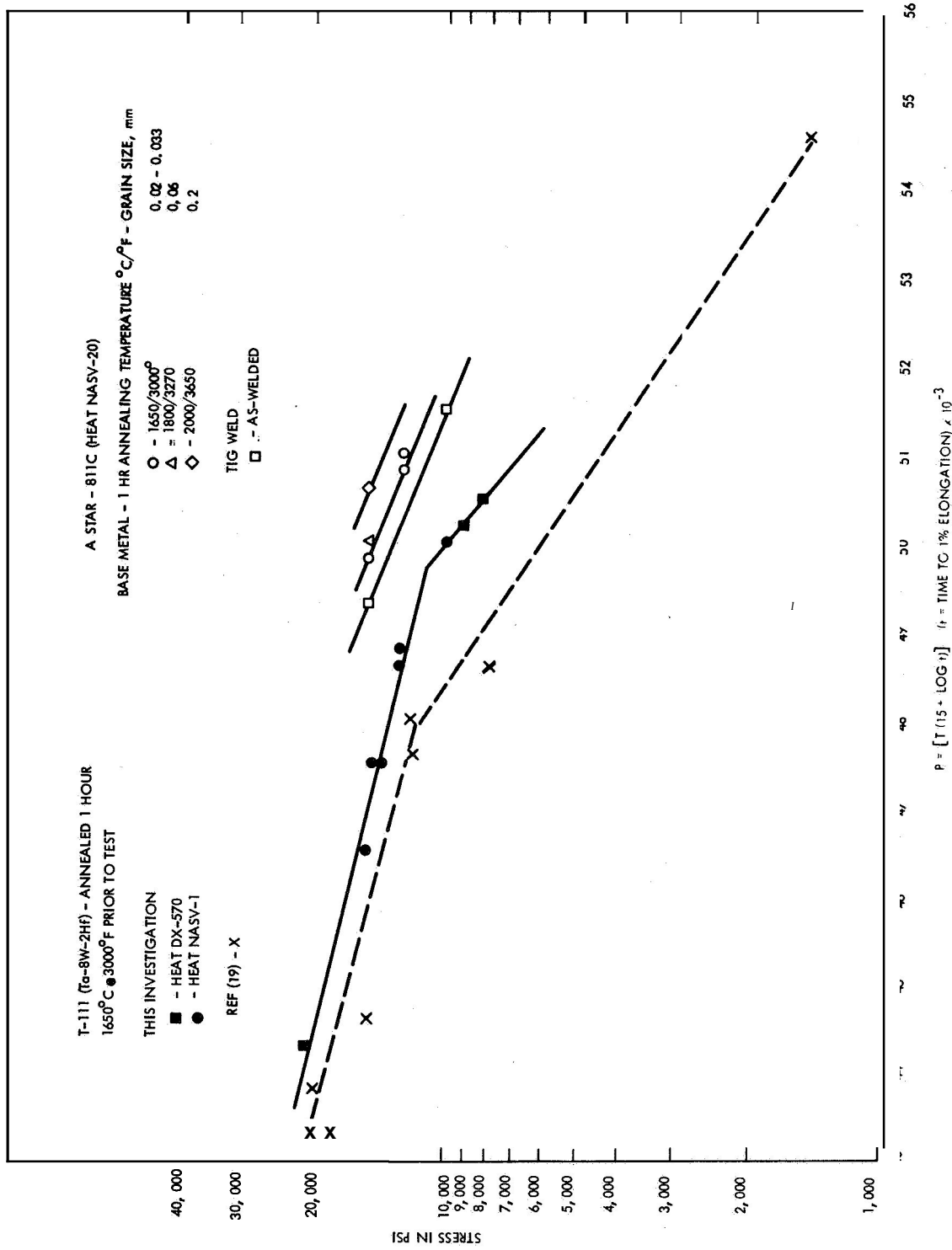


FIGURE 12 - Creep Behavior of ASTAR-811C (Ta-8W-1Re-0.7Hf-0.025C), Heat NASV-20

creep behavior of TIG welded material while outside the scope of this present investigation is nonetheless of vital importance. This behavior will have to be defined since the end item hardware for which these tantalum alloys are being developed will be joined using fusion welding techniques.

b. Tensile Properties. In view of the improvement in creep behavior of composition ASTAR-811C by increasing the pre-test annealing temperature, a study was made to determine the effect of the pre-test annealing temperature on the short time tensile properties. Specimens were annealed for 1 hour at temperatures of 1650, 1800, 2000, and 2200°C (3000, 3270, 3630, and 3990°F) respectively, radiation cooled, and tensile tested at room temperature. Data are recorded in Table 9 and illustrated in Figure 13. As can be seen, the proportional limit and 0.2% yield strength increase with increasing pre-test annealing temperature, while the ultimate strength was unchanged. For the specimen annealed at 2200°C (3990°F), the 0.2% yield strength is 98% of the ultimate strength. Photomacrographs and photomicrographs of the tested specimens are shown in Figure 14. The increase in grain size from 0.020 to 0.400 mm with increasing annealing temperature is very apparent as is the change in precipitate morphology. The increase in yield strength could be due to the additional carbon retained in solution as the annealing temperature was increased, or could be due to the precipitation of coherent carbide during cooling from the solution annealing temperature. The latter view seems more reasonable since the rate of work hardening goes essentially to zero as the annealing temperature was increased to 2200°C and increased rapidly at the lower annealing temperature. This behavior is typical of systems which undergo coherent precipitation hardening.

The mode of fracture appears to change from shear for the specimen annealed at 1650°C (3000°F) to intergranular rupture for the specimens annealed at the higher temperatures. These results are not inconsistent with the failure behavior of ASTAR-811C specimens previously reported¹). With strains of 17 to 25% and reductions in area of 38 to 52%, the mode of failure could hardly be described as brittle, however.

TABLE 9. Room Temperature Mechanical Properties of ASTAR-811C (Heat NASV-20)
as a Function of Pre-test Heat Treatment

Pre-test Heat Treatment (°C)	0.2% Yield Strength (ksi)	Ultimate Tensile Strength (psi)	% Elongation		% Reduction in Area	Proportional Limit (ksi)	DPH	Grain Size (μm)
			Uniform	Total				
1 hr/1650°C furnace cool	83,400	105,400	16.2	24.8	51.9	74,300	258	0.020
1 hr/1800°C furnace cool	84,300	104,600	15.8	23.1	49.2	79,000	260	0.050
1 hr/2000°C furnace cool	90,000	105,300	16.2	23.2	44.7	83,000	262	0.180
1 hr/2200°C furnace cool	103,200	105,000	9.9	18.4	38.4	94,000	279	0.40
1 hr/2000°C helium quench	102,700	108,800	10.8	17.0	46.4	97,000	289	~ 0.180

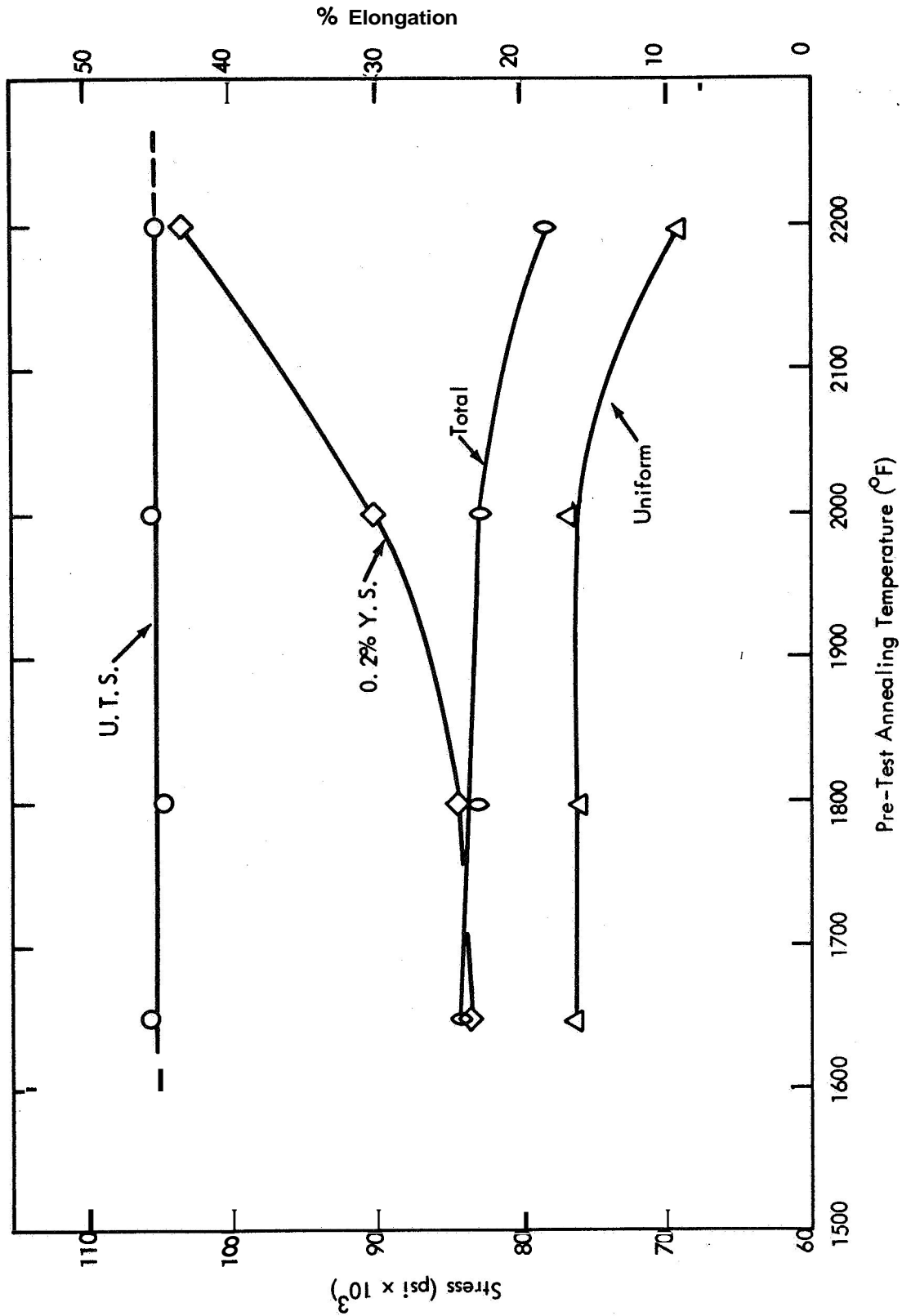
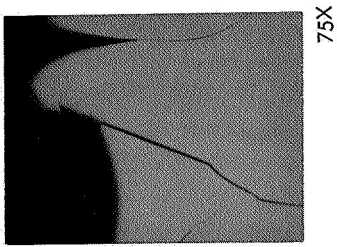
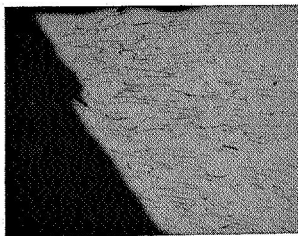


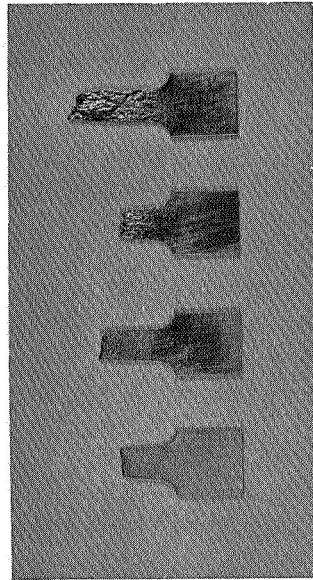
FIGURE 13 - Room Temperature Mechanical Properties of NASV-20 (Ta-8W-1Re-0.7Hf-0.025C) as a Function of Heat Treatment



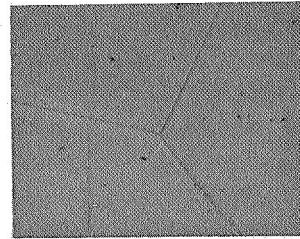
75X



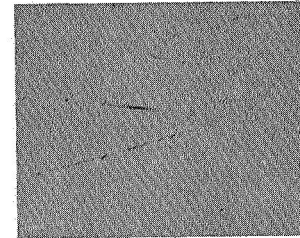
75X



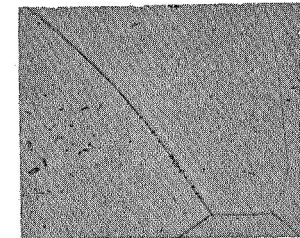
75X



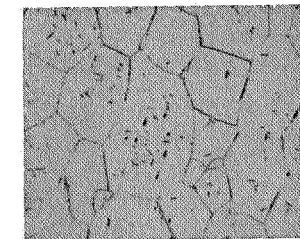
500X



500X



500X



500X

FIGURE 14 - Macro and Microstructure of R. T. Tensile Specimens of NASV-20 (Ta-8W-1Re-0.7Hf-0.025C) Annealed for 1 Hour at 1650, 1800, 2000, and 2200°C Respectively Prior to Testing

2 Metallography of TIG Welded Tensile Test Specimens

Tensile properties were determined on longitudinal and transverse TIG welded 0.04 inch ASTAR-811C sheet specimens over the temperature range of -195°C (-320°F) to 1415°C (2600°F). The tensile data which have been reported previously⁽¹⁾ are repeated in Table 10. The fracture area of the test specimens was examined metallographically and the general appearance and mode of fracture are shown in Figure 15 for specimens tested at -195°C (-320°F) and at room temperature. As would be expected from the tensile data, necking of the transverse welded specimens occurred in the base metal on both sides of the weld and failure eventually occurred in one of these two regions. The intergranular mode of fracture was identical to that previously observed for ASTAR-811C at these temperatures. Fairly uniform elongation occurred within the longitudinally welded specimens, the gage lengths of which consisted entirely of weld and heat affected metal. The deformation of the large as-cast grains resulted in the typical "orange peel" macrostructure shown in Figure 15. As can be seen, the longitudinally welded specimens tested at -195°C (-320°F) and room temperature exhibited intergranular and shear modes of failure respectively.

Of particular interest was the microstructure of the two specimens tested at -195°C (-320°F) at a uniform strain rate of 0.05 inch/inch/minute. During testing of these two specimens, audible clicks, indicative of mechanical twinning, had been heard. Discontinuities in the stress-strain curves were also observed. That mechanical twinning had indeed occurred in both specimens was established metallographically, as shown in Figure 16. However, twinning was much more prevalent in the longitudinally welded specimen. Twins having both smooth sides and irregular sides, similar to Neumann bands in iron, were observed. The extension of twins across grain boundaries is clearly illustrated in Figures 16a and e, while the intersection of twins with each other is shown in Figures 16c and d. Figure 16f indicates the crystallographic nature of the twinning, which most likely occurred on 112 planes, which are the twinning planes in body centered cubic structures. It should be noted that this twinning was solely confined to the weld metal, which had essentially all of the 235 ppm

TABLE 10 Tensile Properties of TIG Welded ASTAR-811C^(a)

Test Temp. (°F)	Weld Direction	0.2% Yield Strength (psi)	Ultimate Tensile Strength(psi)	% Elongation		% Reduction in Area
				Uniform	Total	
-320	Longitudinal	157,300	184,600	16.65	24.20	35.65
-320	Transverse	159,000	176,200	10.90	14.15	41.10
RT	Longitudinal	109,800	115,300	15.0	28.45	48.90
RT	Transverse	89,300	107,200	10.6	18.7	47.8
1800	Longitudinal	44,000	67,100	--	18.7	--
2400	Longitudinal	35,300	41,100	--	29.0	--
2600	Longitudinal	32,500	36,000	--	26.7	--

(a) A constant strain rate of 0.05 inches/minutes used throughout the test

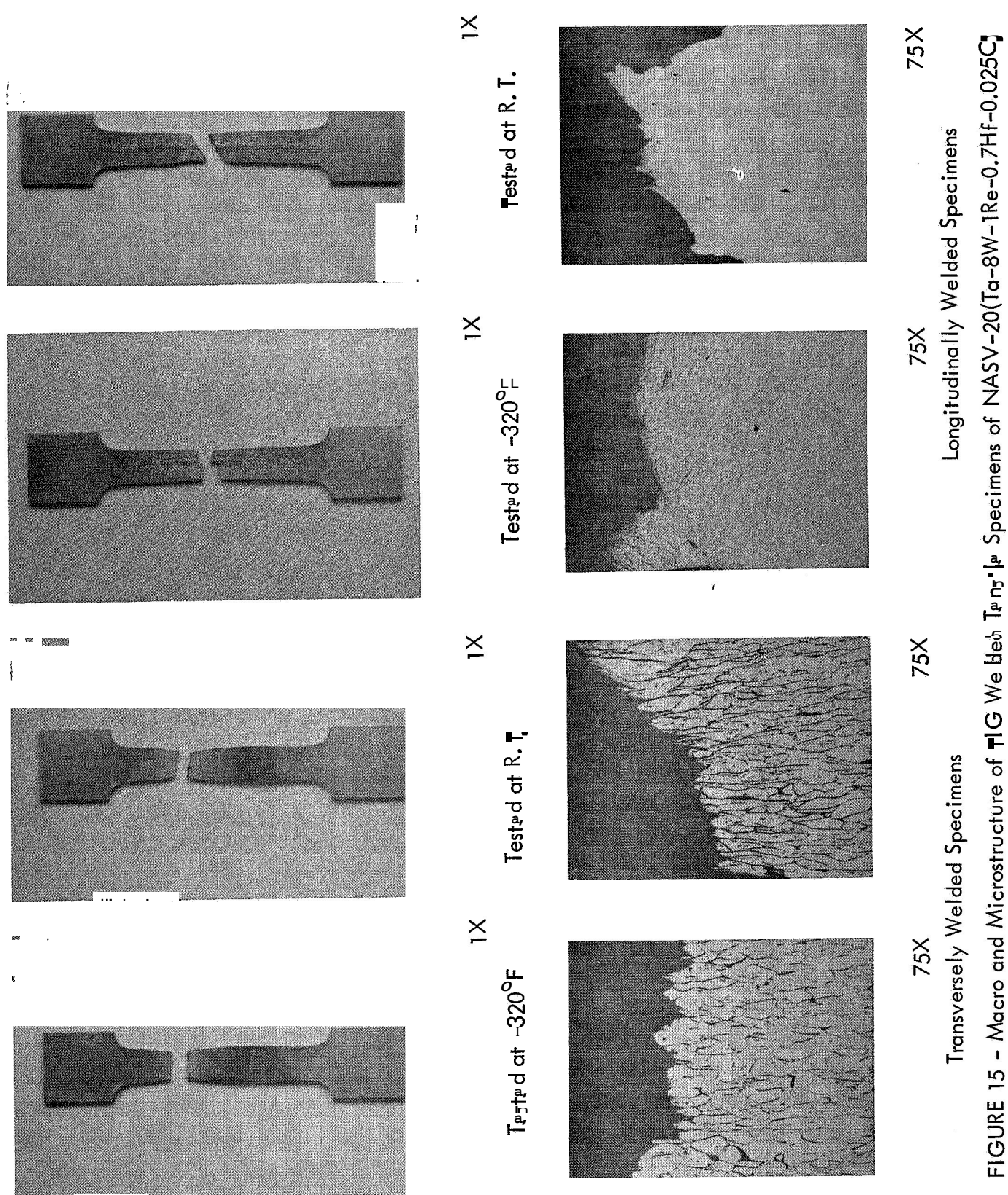


FIGURE 15 - Macro and Microstructure of TIG Welded Specimens of NASV-20(Ta-8W-1Re-0.7Hf-0.025C)

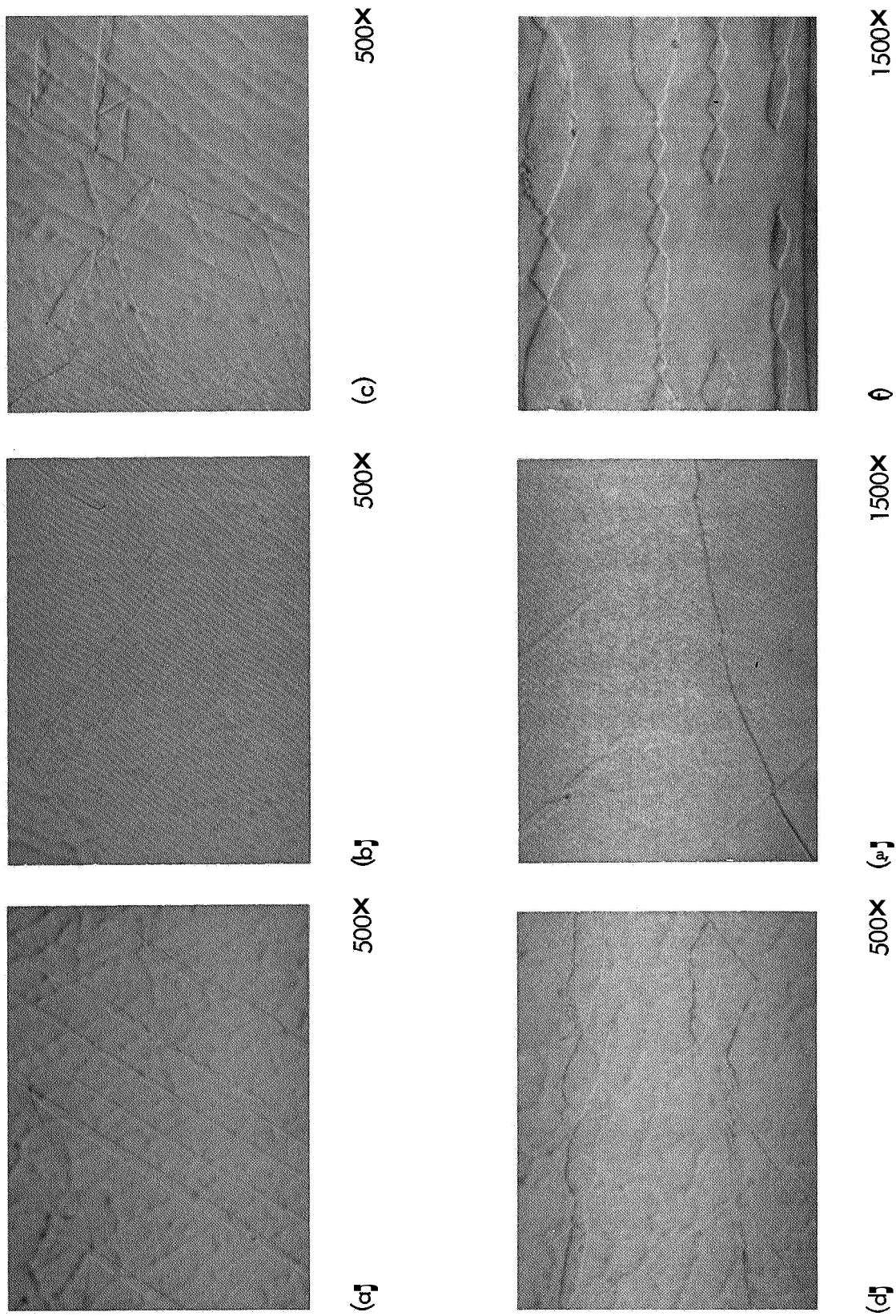


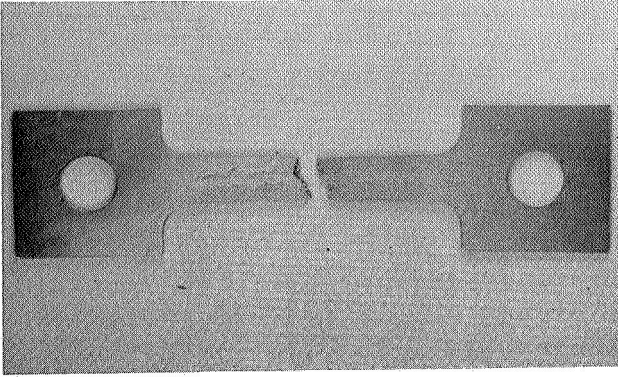
FIGURE 16 - Microstructure of TIG Welded Specimens of NASV-20 (Ta-8W-1Re-4Zr-0.025C) Tested at -320°F, Showing Mechanical Twinning

carbon retained in either solid solution or, as previously discussed, a submicroscopic, possibly coherent precipitate. It also occurred at a temperature just slightly below the transition temperature of the TIG welded material.

Deformation twins have previously been reported in body centered cubic metals. While **Bechtold**⁽⁵⁾ could not induce twinning in tantalum by straining in tension at temperatures as low as that of liquid nitrogen, Barrett and **Bakish**⁽⁶⁾ observed deformation twins in tantalum after impact working at liquid nitrogen temperature. In both studies tantalum of nominal 99.9% purity was used. Anderson and **Bronisz**⁽⁷⁾ induced twinning in electron beam melted tantalum at room temperature and interpreted the results as suggesting that the ease of twin formation in tantalum is enhanced by increasing the purity. This interpretation is in contrast to the results reported here and to those reported by Tipper and **Hall**⁽⁸⁾ and Zow and **Fenstel**⁽⁹⁾ for alpha iron, at least with respect to carbon, nitrogen, and silicon. Similar twinning has also been reported in columbium by Adams, et al⁽¹⁰⁾ and by **Wessel**, France, and Begley⁽¹¹⁾.

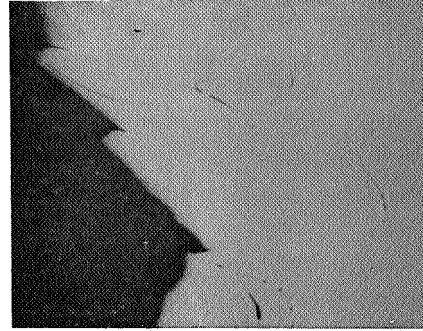
Of interest here is that the twins produced in the tantalum alloy in tension (Figure 16) are similar to those produced in columbium tested in compression.

The general appearance and the fracture mode of longitudinally welded specimens tested in tension at 982, 1316, and 1427°C (1800, 2400, and 2600°F) are shown in Figure 17. The macrostructure of these specimens is quite similar to those tested at the lower temperatures. However, the fracture modes vary somewhat. Failure occurred by shear in the specimen tested at 982°C (1800°F), while a combination of shear and intergranular failures occurred in the specimens tested at 1316 and 1427°C (2400 and 2600°F). The microstructure of these specimens at higher magnifications is illustrated in Figure 18. The wedge-shaped cavities observed in the specimens tested at the two highest temperatures are indicative of elevated temperature grain boundary sliding, and are similar in appearance to those previously found in unwelded specimens of composition **ASTAR-811C** tested in tension at the same temperature. Subgrain boundary formation and the fine matrix precipitation shown in Figure 18 occurred in all three specimens during testing at temperature, even though they were held at temperature for no more than 1 hour.

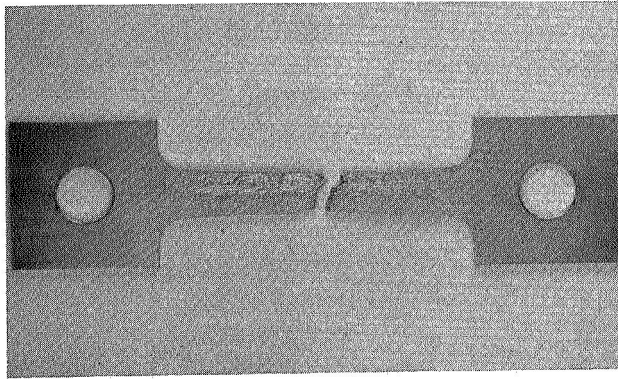


1X

Tested at 2600°F

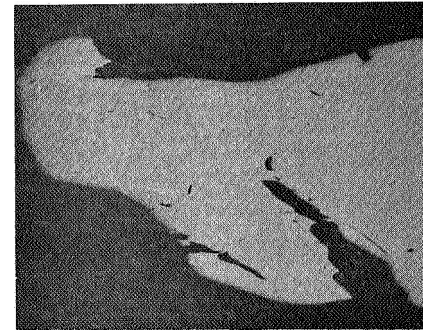


50X

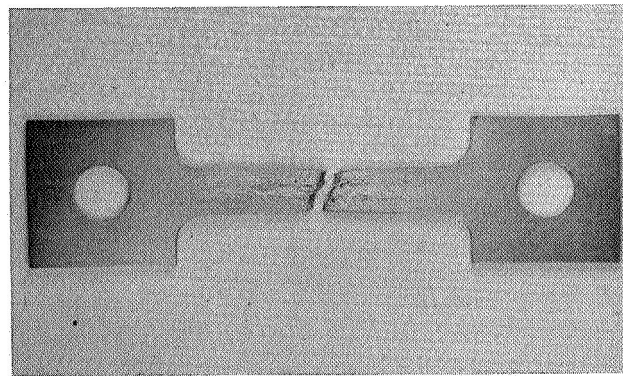


1X

Tested at 2400°F

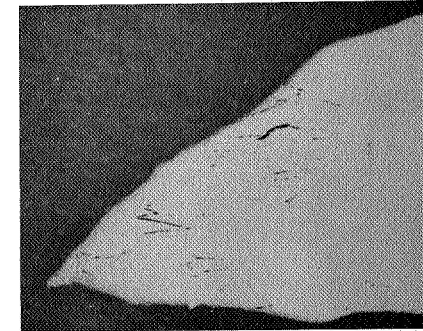


50X



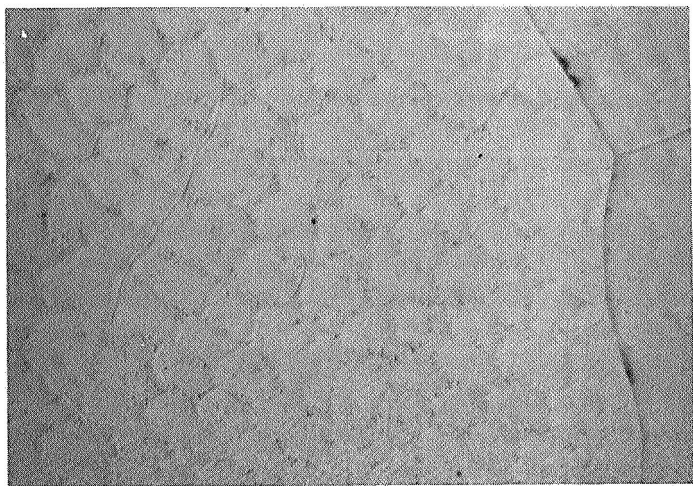
1X

Tested at 1800°F

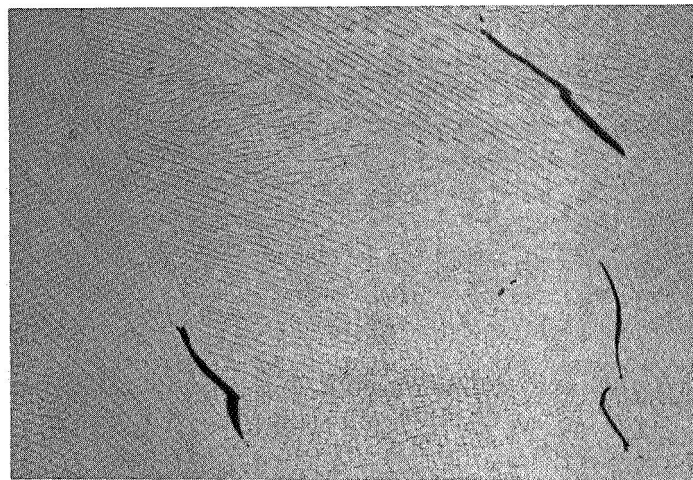


50X

FIGURE 17 - Macro and Microstructure of TIG Welded Tensile Specimens of NASV-20(Ta-8W-1Re-0.7Hf-0.025C



(c) Structure Typical of Specimens
Tested at 1800, 2400, & 2600°F
500X



(b) Tested at 2600°F
100X



(a) Tested at 2400°F
100X

FIGURE 18 - Microstructure of TIG Welded Tensile Specimens of NASV-20(Ta-8W-1Re-0.7Hf-0.025C)
Tested at Elevated Temperature

C. PHASE IDENTIFICATION AND MORPHOLOGY

Increasing the final annealing temperature of ASTAR-811C from 1650°C (3000°F) to 2000°C (3632°F) resulted in significant increases in creep resistance and short time yield strength.

Phase identification and morphology studies were initiated on as heat treated and as heat treated and tested material in order to determine the reasons for the differences in both the short time tensile and long time creep behavior. The results will be completed and reported in a later quarterly progress report.

III. FUTURE WORK

During the next quarterly period it is planned to accomplish the following.

1. Continue evaluation of creep properties of ASTAR-811C.
2. Complete the phase identification and morphology studies on composition ASTAR-811C creep specimens.
3. Fabricate the electrodes of the compositions to be scaled up to 4-inch diameter size. These electrodes will then be melted into ingots, and processing to 0.04-inch sheet **will** be initiated.

IV. REFERENCES

1. R. W. Buckman, Jr., and R. C. Goodspeed, "Development of Dispersion Strengthened Tantalum Base Alloy", 9th Quarterly Progress Report, WANL-PR(Q)-010.
2. G. G. Lessmann and D. R. Stoner, "Determination of the Weldability and Elevated Temperature Stability of Refractory Metal Alloys", 8th Quarterly Progress Report, WANL-PR(P)-008.
3. D. Rowcliffe et al, "Strengthening of Niobium-Zirconium Alloys by Internal Oxidation" Presented at Conference on Oxide Dispersion Strengthening, Bolton Landing, New York, June 27-29, 1966.
4. R. W. Buckman, Jr., and R. T. Begley, "Development of Dispersion Strengthened Tantalum Base Alloy", Final Technical Report, Phase I, WANL-PR(Q)-004.
5. D. Hanson, "The Creep of Metals", Trans. AIME, Vol. 133, 1939, p. 15.
6. C. Crussard, "The Influence of Grain Size on Creep Rate", Comptes rendus, Vol. 219, 1944, p. 681.
7. P. Shahinian and J. R. Lane, "Influence of Grain Size on High Temperature Properties of Monel", Trans. ASM, Vol. 45, 1953.
8. F. Garafalo, "Fundamentals of Creep and Creep-Rupture in Metals", MacMillan Series in Materials Science, 1965.
9. P. Feltham and J. D. Meakin, Acta Met, 7, 614, 1959.
10. J. McKeown, J. Inst. Metals, 60, 201, 1937.
11. R. T. Begley and J. Cornie, "Development of Columbium Base Alloys", 5th Quarterly Progress Report, Contract AF 33(615)-1728 (WANL-PR(U)-021, March 15, 1966.
12. J. H. Bechtold, Acta Met. 3, 249 (1955).
13. C. S. Barrett and R. Bakish, Trans. Amer. Inst. Min. (Metall.) Engrs. 212, 122 (1958).
14. R. W. Anderson and S. E. Bronisz, Acta Met. 7, 645 (1959).
15. C. F. Tipper and E. O. Hail, J. Iron St. Inst. 175, 9 (1953).

IV. REFERENCES (CONTINUED)

16. J. R. Low and R. G. Feustel, Acta Met. 1, 185 (1953).
17. M. A. Adams, A. C. Roberts, and R. E. Smallman, Acta Met. 8, 328 (1960).
18. E. T. Wessel, L. L. France, and R. T. Begley, in Columbium Metallurgy, Interscience, New York-London, 1961, p. 459.
19. J. Sawyer and E.A. Steigerwald, "Generation of Long Time Creep Data of Refractory Metal Alloys at Elevated Temperature", 12th Quarterly Progress Report, NASA-CR-72044, NASA Contract 3-2545.
20. R. W. Buckman, Jr. , "Development of Dispersion Strengthened Tantalum Base Alloy", 4th Quarterly Progress Report, WANL-PR-(Q)-005, NASA-CR-54288.
21. R. W. Buckman, Jr. , "Development of Dispersion Strengthened Tantalum Base Alloy", 5th Quarterly Progress Report, WANL-PR-(Q)-006, NASA-CR-54462.
22. G. G. Lessmann and D. R. Stoner, "Determination of the Weldability and Elevated Temperature Stability of Refractory Metal Alloys", 7th Quarterly Progress Report, WANL-PR(P)-007, NASA-CR-54434.
23. R. L. Fleischer and W. R. Hibbard, Jr. , "Solution Hardening", p. 261, The Relation Between the Structure and Mechanical Properties Metals, Vol I, Symposium No. 15, London: Her Majesty's Stationery Office, 1963.
24. L. L. Seigle, "Solid Solution Strengthening of Refractory Metals", Agard Conference on Refractory Metals. Oslo University Centre - Oslo- Blindern, Norway, June 23-26, 1963.

APPENDIX I

RECOMMENDATIONS FOR SELECTION OF COMPOSITIONS FOR MELTING AS, FOUR-INCH DIAMETER INGOTS

In accordance with the Phase II Work Statement, Contract NAS 3-2542, WANL is to melt three (3) tantalum alloy compositions as 4-inch diameter ingots, each weighing approximately 60 pounds. Each ingot is to be processed to sheet and evaluated with regard to creep strength, fabricability and weldability. The commercially available high strength tantalum base alloys T-111 and T-222 are being used as the reference standard.

Theoretical considerations indicate that neither hafnium nor zirconium, as a substitutional solute addition, would be expected to enhance the creep behavior of tantalum. However, the addition of a reactive metal to tantalum is necessary to impart corrosion resistance to liquid alkali metals. One atom per cent reactive metal gives columbium base alloys the necessary liquid alkali metal corrosion resistance, viz Cb-1Zr ; thus, it was assumed that tantalum base alloys would behave in an analogous manner. Therefore, the level of reactive metal addition (Hf or Zr) was limited to nominally one atom per cent.

Interaction of the intentional C and/or N addition will result in the desired HfC , HfN , and/or Hf(CN) dispersed second phase. Corrosion data for D-43 indicate that the liquid alkali metal corrosion resistance imparted by the zirconium is maintained even if the zirconium exists in a combined form (i.e., ZrC) and that the ZrC is stable in contact with liquid alkali metals. There are no data available on the stability of the HfN in liquid alkali metals, and although we have assumed that the behavior will be no different than the carbides, investigation of the nitride stability in liquid alkali metals is needed.

The initial four-inch diameter composition, Ta-8W-1Re-1Hf-0.025C (NASV-20) selected with the cognizance of the NASA project manager was chosen as a straight carbide strengthened composition which exhibited significantly better creep resistance than T-222 while retaining the fabricability and weldability characteristics intermediate to those of T-111 and T-222. The selection of NASV-20 was made after analysis of the data generated during the Phase I portion of the investigation. Briefly, in the Phase I portion of the investigation, the Ta-W-Hf-C system was studied to determine the substitutional

(W + Hf) — interstitial (carbon) solute level which provided improved creep resistance with minimal loss in low temperature ductility. The results summarized in Table I show that 9 to 10 a/o W + Hf with up to 350 ppm carbon can be added to tantalum without seriously compromising fabricability while significantly improving creep resistance. The effects of Mo and Re, Zr, and N substitution for a portion of the W, Hf, and carbon respectively was studied using the Ta-8W-(0.5-1)Hf-(0.02-.07)C composition. A statistically designed experiment was used to reduce the number of compositions required for evaluation. Substitution of up to 1.5 Mo for an equivalent amount of W or substituting Zr for hafnium did not cause any significant change in either fabricability or mechanical properties. However, substitution of Re for W resulted in a significant improvement in creep properties, without affecting weldability or short time mechanical properties (see Table 2). At rhenium contents above 1 a/o, little additional improvement in creep resistance is realized, with the most significant effect of rhenium on creep resistance occurring at the 0.5 to 1 a/o level (see Figure 1). The beneficial effect of interstitials on the creep behavior of a Ta-W-Re-Hf matrix is apparent from the data shown in Figure I-1.

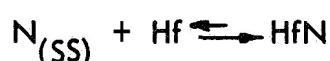
The interstitial species added to interact with the reactive metal addition (Hf) has a significant effect on the creep behavior (see Figure I-2) of the tantalum alloy matrix. The addition of carbon to a Ta-W-Hf or Ta-W-Re-Hf matrix results in a significant improvement in creep behavior. However, substituting a portion of the C with N results in a still further improvement in creep resistance. The more effective strengthening of the N addition at the higher (≥ 400 ppm) level is attributed to the precipitation morphology and kinetics of the Hf, Zr, N dispersoid. Analysis of the dispersed second phases extracted from creep specimens and from specimens used to study heat treat response led to the following conclusions.

- (1) In the straight carbide strengthened system (NASV-20) the principal precipitation reaction is



The relatively low carbon solubility in the tantalum alloy matrix (~ 150 ppm at 3000°F), and the relatively fast precipitation kinetics results in a carbide precipitate along high angle and sub-boundaries during cooling from the heat treatment temperature. The higher the final annealing temperature, the finer the resulting precipitate. Thus, heat treatment can be used to effectively control final structure, and creep is a structure sensitive property.

(2) In the Ta-W-Re-Hf-N system, the principal precipitation reaction is



Nitrogen has a high solid solubility in unalloyed Ta (4400 ppm at 1200°C) and also exhibits an apparent high solubility in the Ta-W-Re-Hf alloy matrix. The sluggishness of the precipitation reaction at low N_2 concentrations (≤ 300 ppm) and the formation of a coherent precipitate give interesting strength properties but result in sheet and/or tubing fabrication difficulties which will be discussed later. The advantage of nitrogen as a strengthening addition is achieved at the higher N_2 levels, > 400 ppm, where response to classical age hardening has been observed. Overaging occurs at $2300\text{--}2500^{\circ}\text{F}$ with the maximum hardness occurring after heating for one hour at $2000\text{--}2200^{\circ}\text{F}$. Thus, age hardenable tantalum-nitrogen alloys show particular potential for use as bar-or forged components such as required in rotating parts of a turbogenerator.

The sluggishness of the HfN precipitation reaction can, however, be effectively utilized by substituting a portion of the carbon with N_2 at levels (< 200 ppm) where fabricability would not be seriously compromised but where additional improvement in creep strength is realized. The fast precipitating carbide phase stabilizes the substructure while the more sluggish precipitating nitride phase apparently provides additional enhancement of long time creep properties (see Figure 3).

Fabricability and weldability characteristics will limit the alloying additions to a level which will permit processing an as-cast ingot to sheet and/or tubing. The standard for weldability and fabricability is T-111 (Ta-8W-2Hf). As-cast T-111 ingots can be broken

down by forging and/or extrusion at 2000–2400°F and secondary working (sheet rolling and/or tubing drawing) can be done at ambient temperature utilizing existing commercial technology. The apparent high nitrogen solubility in the tantalum alloy matrix limits the level of interstitial which can be added before fabricability is impaired. The data plotted in Figure 4 shows the effect of C and N on the room temperature hardness of a Ta-(8-9) W-(0.5-1) Hf matrix and of N on a Ta-9W-1.5Re-1Hf matrix. The apparent high N solubility results in essentially a linear increase in room temperature hardness with increasing N content. Generally, tantalum base alloys with a room temperature hardness in excess of approximately 300 DPH are difficult to fabricate to sheet. A Ta-9W-1.5Re-1Hf-0.03N composition (R. T. hardness 370 DPH) while forgeable could not be rolled to sheet at 800°F. The low carbon solubility results in a significant initial hardness increase similar to that for N, but as the solubility limit is exceeded there is little further hardness increase as the non-coherent carbide precipitates.

Weldability, evaluated by measuring the change in the bend ductile-brittle transition temperature for as TIG welded material, is sensitive to the substitutional and interstitial solute level. For a matrix containing 9-12 w/o W + Re + Mo + Hf, C + N additions above 200 ppm cause a rapid increase in the DBTT with N generally causing a slightly greater rate of change (see Figure 5).

The carbo-nitride has been shown to be more effective in enhancing creep properties than the straight carbide, and at a level of 300 ppm C + N, excellent creep properties are obtained, while retaining adequate fabricability with a 9-12 w/o W + Re + Mo + Hf matrix. At a nominal 300 ppm C + N, a linear relationship between the DBTT and the square root of the tungsten equivalent* atom per cent was observed (see Figure 6).

A final criteria for evaluation of the promising alloy composition was the long time thermal stability and tolerance for oxygen contamination. The test procedure used simulates a

*tungsten equivalent = %W + %Mo + %Hf + 3 x %Re

highly specific set of conditions and here again, the basis for comparison is T-111. The results are summarized in Table 3. T-111 is apparently more tolerant of O₂ contamination than the more creep resistant complex tantalum base alloys. However, the rate of change in DBTT with O₂ contamination was less for the carbo-nitride strengthened alloy than for the rhenium containing solid solution strengthened compositions (NASV 19 and 21). The carbide strengthened composition (NASV-20) though containing 250 ppm carbon behaved essentially identical to the solid solution strengthened compositions (NASV-19, 21).

Since structure has been shown to exert the most significant effect on creep properties, fabricability will limit the substitutional and interstitial solute level. Creep strength at any given solute level can be controlled by thermal treatment. Thus, the second four-inch diameter ingot composition recommended for melting is Ta-6.5W-1Re-0.85Hf-0.015C-0.015N. The substitutional solute level was selected to give an as-welded DBTT near -100F.

The data generated do not justify selection of a third dispersed phase strengthened composition. Thus, it is recommended that more detailed investigation of thermal-mechanical treatment and its effect on properties be conducted in lieu of melting a third ingot.

TABLE I

W + Hf %	Carbon ppm	Fabricability	Weldability	Creep Strength
6	500 1000	1 2	1 3	4 5
9	200 350	1 1	1 2	1 1
10 (T-111)	-	1	1	3
12	450 900	3 4	5 5	- -
12 - 14 (T-222)	100	2	2	2
15	0 300	3 5	5 -	- -

<u>Relative Ranking</u>	<u>Fabricability</u>	<u>Weldability</u>	<u>(2400°F) Creep Strength</u>
1 - Excellent	T-111	DBTT << R. T.	> T-222
2 -	T-222	--	T-222
3 - Moderate	-	DBTT — R. T.	~T-111
4 -	-	--	--
5 - Poor	-	DBTT >> R. T.	--

TABLE 2
Effect of Re on Properties^(a) of Ta-W-Hf-C Alloy

Property	Ta-9W-1Hf-0.025 C (NASV-9)	Ta-8W-1Re-1Hf-0.025C (NAS 56-57)
I. Room Temperature' a) Tensile strength b) 0.2% yield strength c) % elongation Uniform Total	106,800 psi 78,600 psi 15% 24%	105,000 psi 78,000 psi 17% 28%
II. Bend ductile brittle transition temperature for as-TIG welded 0.04-inch sheet, tested over 1.8t bend radius	-125 to -175°F	-100 to -125°F
111. Time to 1% strain at 2400°F and 15,000 psi	108 hours	300 hours

(a) All tests on 0.04-inch thick sheet, annealed for one hour at 3000°F prior test.

TABLE 3
Effect of Oxygen Contamination^(a) on as-TIG Welded
Bend^(b) Ductile-Brittle Transition Temperature

Composition (w/o)	Undoped	DBTT, °F +150 ppm O ₂	+350 ppm O ₂
Mo-7.5W-1.5Re-0.5Hf-0.015C-0.015N (NASV-12)	+100	+26	+400
Ta-6.5W-2.5Re-0.3Hf-0.01C-0.01N (NASV-13)	+100	+36	+450
Ta-5W-1Re-0.3Zr-0.025N (NASV-18)	+550	+75	+400 ⁺
Ta-8.5W-1.5Re-1Hf (NASV-19)	-250	< 0	Failed during Welding
Ta-8W-1Re-0.7Hf-0.025C (NASV-20)	<-250	+75	+300
Ta-10W-1Re-0.5Hf (NASV-21)	-250	+75	+300
Ta-8W-2Hf (T-111)	-320	-300	-100
Ta-10W-2.5Hf-0.01C (T-222)	-250	0	+250
Co-27Ta-10W-1Zr (FS-85) ^(c)	-125	0	+100

(a) O₂ Doped, Stabilized 50 Hrs. at 1800°F Prior to Welding.

(b) T_{DBTT} of as-welded bend specimen

(c) At equivalent atom %

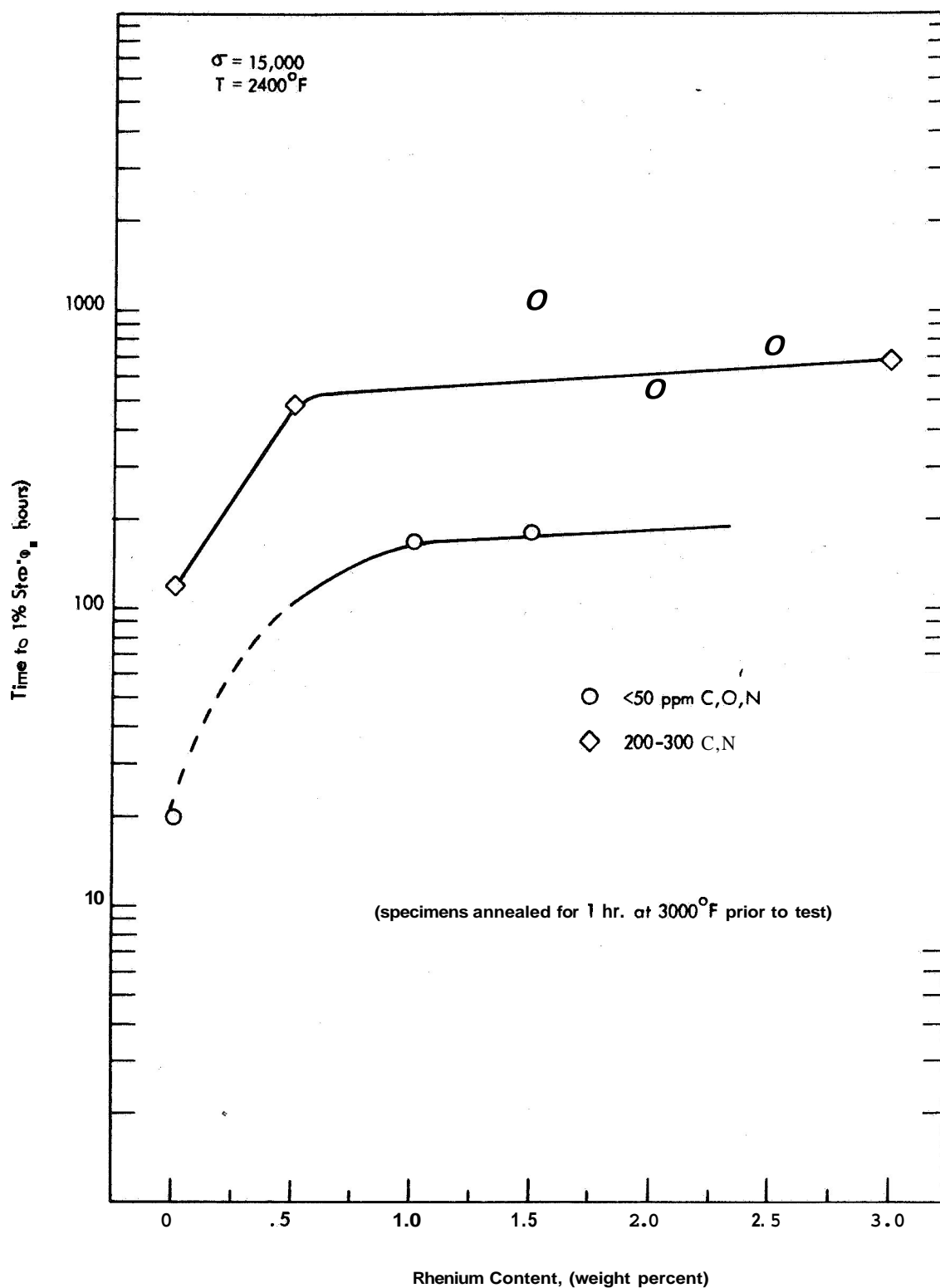


**FIGURE 1 - Effect of Rhenium on Creep Properties of Ta-W-Hf Alloys
(Specimens Annealed 1 Hr. at 3000°F Prior to Test)**

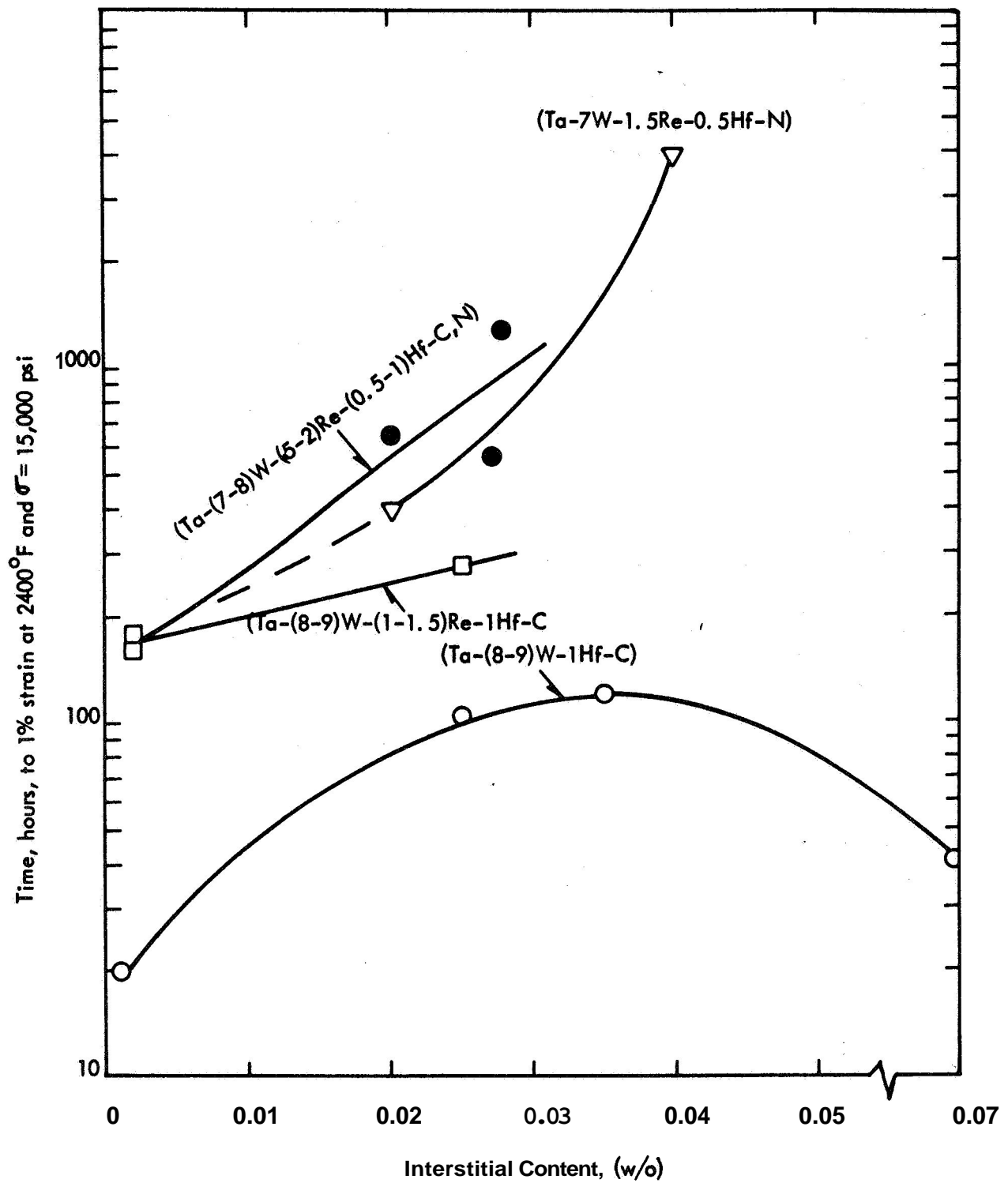


FIGURE 2 - Effect of Carbon and/or Nitrogen on the Creep Behavior of Ta-(7-9)W-(0-2)Re-(0.5-2)Hf Alloy (Specimens Annealed 1 Hr. at 3000°F Prior to Test).

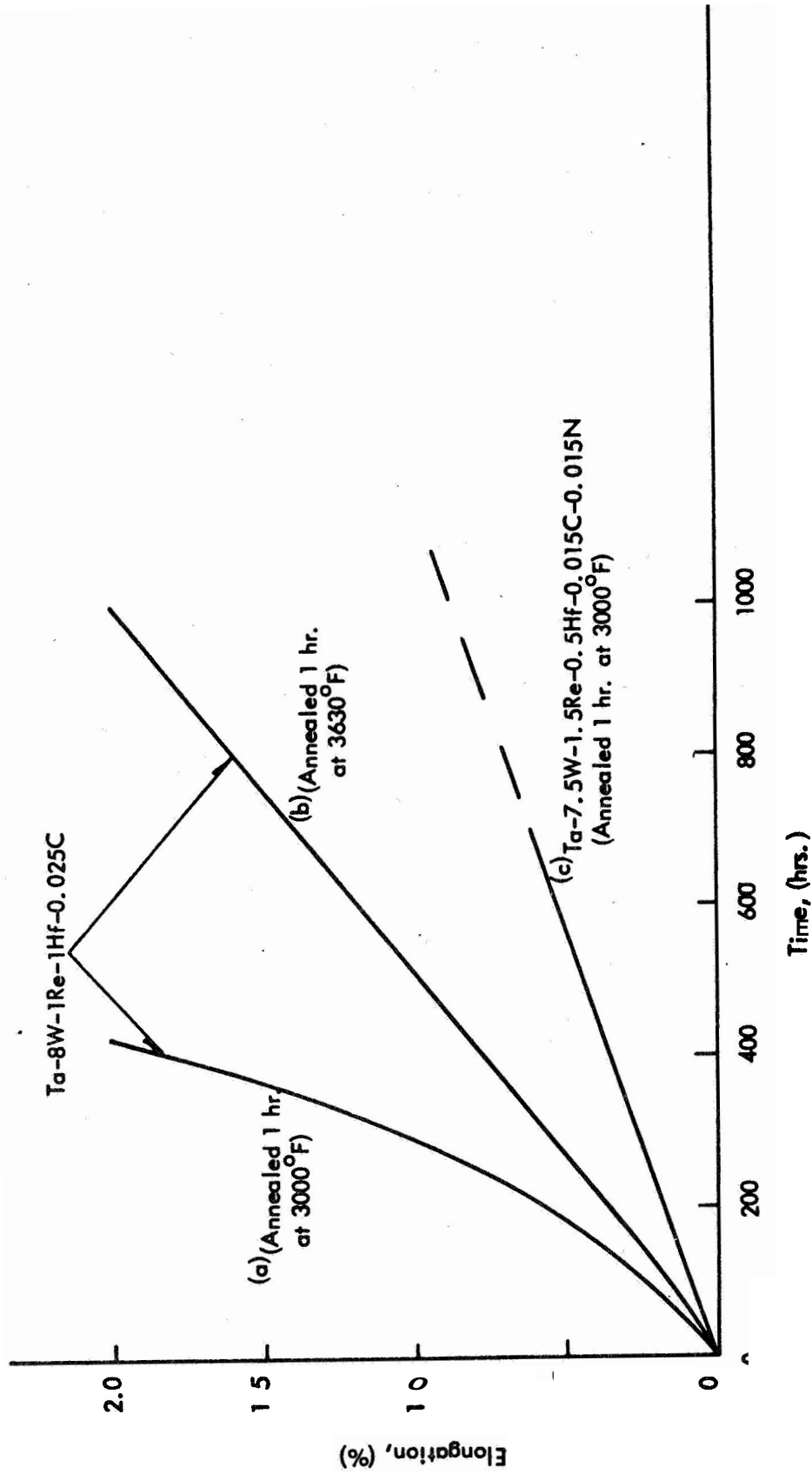


FIGURE 3 - Creep Behavior of Tantalum Base Alloys Tested at 2400°F and 15,000 psi

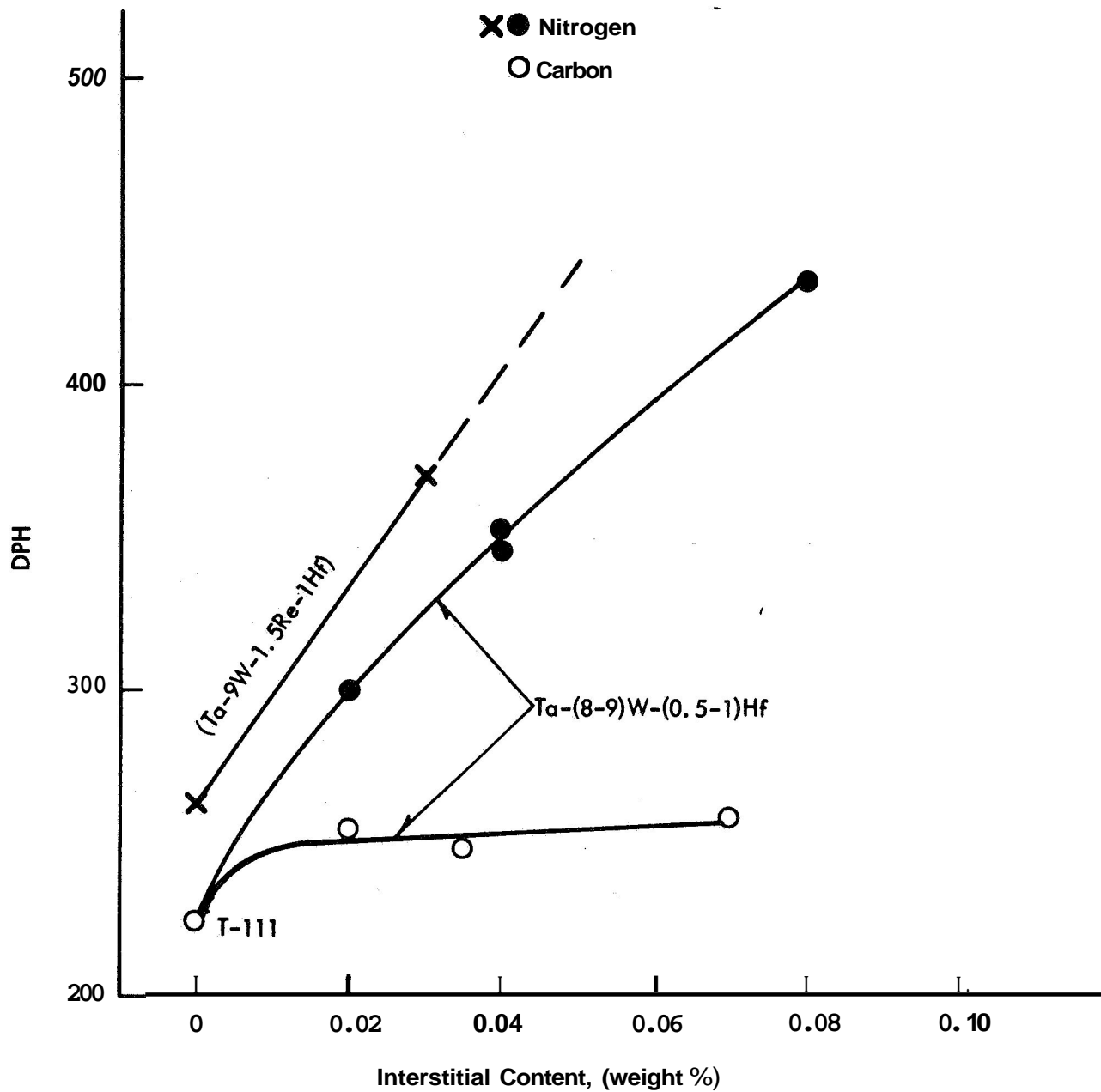


FIGURE 4 - Effect of Carbon and/or Nitrogen on the Room Temperature Hardness of Tantalum Base Alloys.

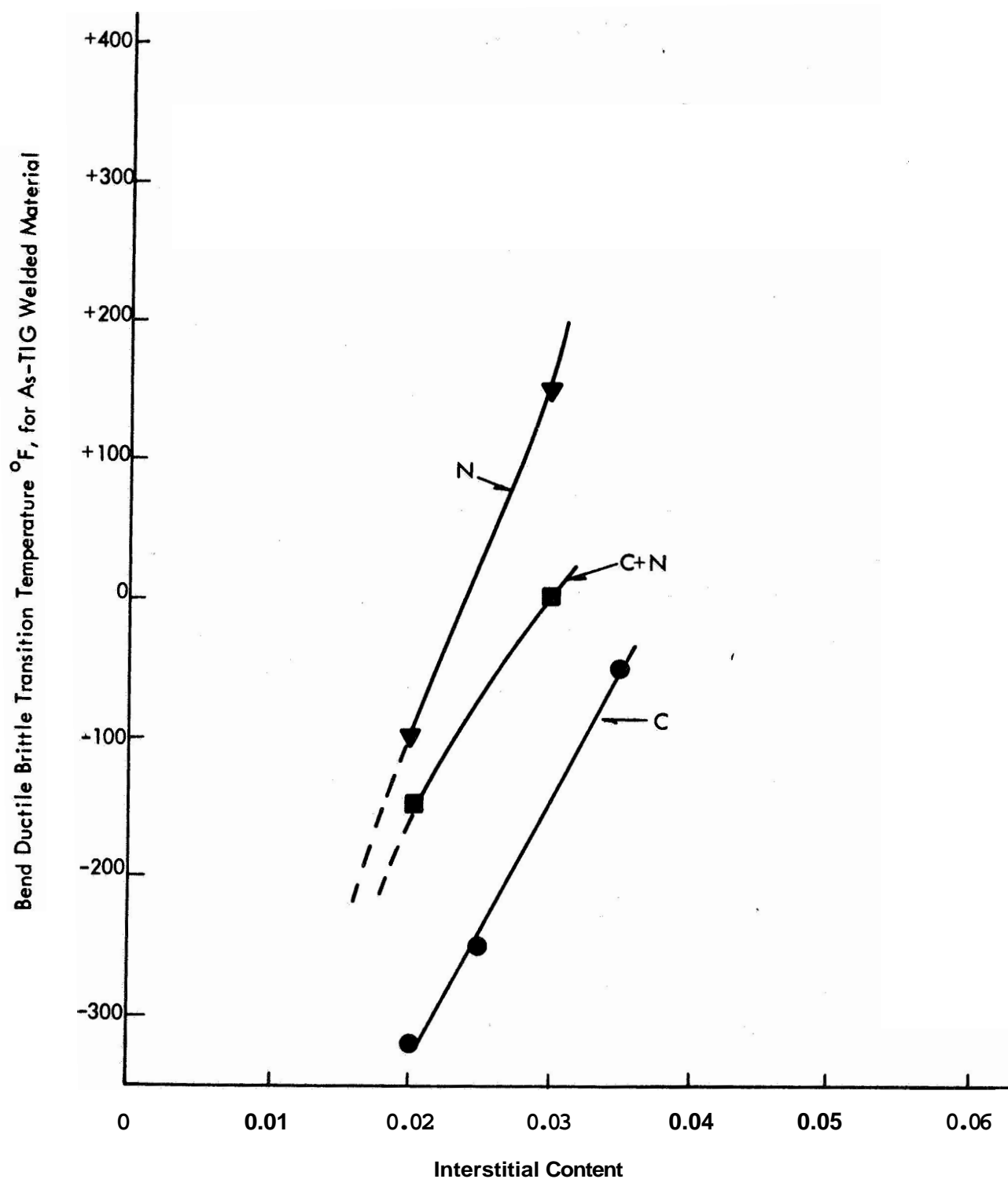


FIGURE 5 - Effect of Carbon and/or Nitrogen on the Bend Ductile Brittle Transition Temperature for As-TIG Welded 0.04 Inch Sheet. (1.8t Bend Radius)

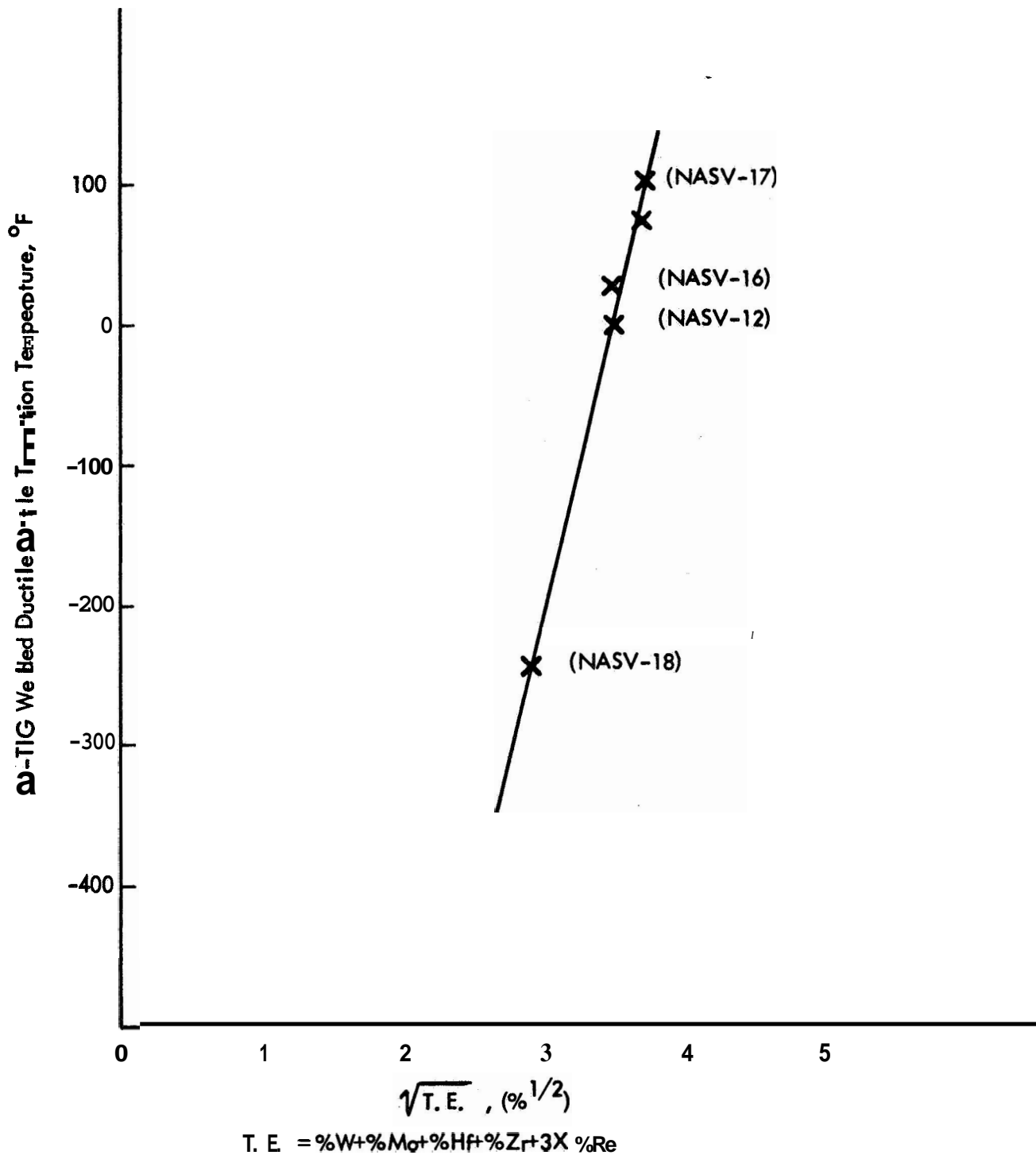


FIGURE 6 - Effect of Substitutional Content on Ductile-Brittle Transition Temperature of As-TIG Welded Ta-W-Re-Mo-Hf Matrix Containing Nominally 300 ppm C+N. (Bend Radius 1.8t)

DISTRIBUTION LIST

TRW

Caldwell Research Center
23555 Euclid Avenue
Cleveland, Ohio 44117
Attn: Librarian
Attn: G. J. Guarnieri

TRW

New Devices laboratories
7209 Platt Avenue
Cleveland, Ohio 44104
Attn: Librarian

National Aeronautics & Space Adm.
Washington, D. C. 20546
Attn: Walter C. Scott
Attn: James J. Lynch (RN)
Attn: George C. Deutsch (RR)
Attn: S. V. Manson

National Aeronautics & Space Adm.
Scientific and Technical Inf. Facility
Box 5700
Bethesda, Maryland 20811

NASA-Ames Research Center
Moffet Field, California 94035
Attn: Librarian

NASA-Goddard Space Flight Center
Greenbelt, Maryland 20771
Attn: Librarian

NASA-langley Research Center
Hampton, Virginia 23365
Attn: Librarian

NASA-Manned Spacecraft Center
Houston, Texas 77001
Attn: Librarian

NASA-Jet Propulsion Laboratory
4800 Oak Grove Drive
Pasadena, California 91103
Attn: Librarian

NASA-Lewis Research Center
21000 Brookpark Road
Cleveland, Ohio 44135
Attn: Librarian
Attn: Dr. Bernard Lubarsky
Attn: Mr. Roger Mather
Attn: Mr. G.M. Ault
Attn: Mr. J. Joyce
Attn: Mr. P. E. Moorhead
Attn: Mr. N.T. Musial
Attn: Mr. T. Strom
Attn: Mr. T. A. Moss
Attn: Dr. Louis Rosenblum
Attn: J. Creagh
Attn: Mr. J. Dilley
Attn: Mr. G.K. Watson
Attn: Mr. T. Moore
Attn: Mr. G. Tulsia
Attn: Mr. W. D. Klopp
Attn: Mr. C. Hoffman
Attn: NASA-Lewis lab. Report Central
Section

NASA- Western Operations Office
150 Pico Boulevard
Santa Monica, California 90406
Attn: Mr. John Keeler

National Bureau of Standards
Washington 25, D. C.
Attn: Librarian

NASA-George C. Marshall Space Flight Center
Huntsville, Alabama 35812
Attn: Librarian
Attn: Wm. A. Wilson



Aeronautical Systems Division
Wright-Patterson Air Force Base, **Ohio**
Attn: Charles Armbruster
Attn: T. Cooper
Attn: Librarian
Attn: John L. Morris
Attn: H. J. Middendorp

Army Ordnance Frankford Arsenal
Bridesburg Station
Philadelphia 37, Pennsylvania
Attn: Librarian

Bureau of Ships
Dept. of the Navy
Washington 25, D. C.
Attn: Librarian

Bureau of Weapons
Research and Engineering
Material Division
Washington 25, D. C.
Attn: Librarian

U. S. Atomic Energy Commission
Technical Reports Library
Washington 25, D. C.
Attn: J. M. O'Leary

U. S. Atomic Energy Commission
Germantown, Maryland
Attn: Col. E. L. Douthett
Attn: H. Rothen
Attn: Major Gordon Dicker

U. S. Atomic Energy Commission
Technical Information Service Extension
P. O. Box 62
Oak Ridge, Tennessee

U. S. Atomic Energy Commission
Washington 25, D. C.
Attn: M. J. Whitman

Argonne National Laboratory
9700 South Cross Avenue
Argonne, Illinois
Attn: Librarian

Brookhaven National Laboratory
Upton, Long Island, New York
Attn: Librarian

Oak Ridge National Laboratory
Oak Ridge, Tennessee
Attn: W. O. Harms
Attn: Dr. A. J. Miller
Attn: Librarian
Attn: N.T. Bray

Office of Naval Research
Power Division
Washington 25, D. C.
Attn: Librarian

U. S. Naval Research Laboratory
Washington 25, D. C.
Attn: Librarian

Advanced Technology Laboratories
Division of American Standard
369 Whisman Road
Mountain View, California
Attn: Librarian

Aerojet General Corporation
P. O. Box 296
Azusa, California
Attn: Librarian

Aerojet General Nucleonics
P.O. Box 77
San Ramon, California
Attn: Librarian

AiResearch Manufacturing Company
Sky Harbor Airport
402 South 36th Street
Phoenix, Arizona
Attn: Librarian
Attn: E. A. Kovacevich

AiResearch Manufacturing Company
9851-9951 Sepulveda Boulevard
Los Angeles 45, California
Attn: Librarian

I. I. T. Research Institute
10 W. 35th Street
Chicago, Illinois 60616

Atomics International
8900 DeSoto Avenue
Canoga Park, California 91304
Attn: W. Botts

Avco
Research & Advanced Development Dept.
201 Lowell Street
Wilmington, Massachusetts
Attn: Librarian

Babcock and Wilcox Company
Research Center
Alliance, Ohio
Attn: Librarian

Battelle Memorial Institute
505 King Avenue
Columbus, Ohio
Attn: C. M. Allen
Attn: Librarian
Attn: Defense Metals Inf. Center

The Bendix Corporation
Research Laboratories Division
Southfield, Detroit 1, Michigan
Attn: Librarian

Bell Aerosystems Co.
P.O. Box 1
Buffalo 5, New York
Attn: E. J. King

The Boeing Company
Seattle, Washington
Attn: Librarian

Brush Beryllium Company
17876 St. Clair Avenue
Cleveland, Ohio 44110
Attn: Librarian

Carborundum Company
Niagara Falls, New York
Attn: Librarian

Chance Vought Aircraft Inc.
P. O. Box 5907
Dallas 22, Texas
Attn: Librarian

Clevite Corporation
Mechanical Research Division
540 East 105th Street
Cleveland 8, Ohio
Attn: Mr. N. C. Beerli

Climax Molybdenum Company of Michigan
1600 Huron Parkway
Ann Arbor, Michigan
Attn: Librarian

Convair Astronautics
50001 Kerny Villa Road
San Diego 11, California
Attn: Librarian

E. I. duPont de Nemours and Co., Inc.
Wilmington 98, Delaware
Attn: Librarian

Electro-Optical Systems, Inc.
Advanced Power Systems Division
Pasadena, California
Attn: Librarian

Fansteel Metallurgical, Corp.
North Chicago, Illinois
Attn: Librarian



Ford Motor Company
Aeronutronics
Newport Beach, California
Attn: Librarian

General Dynamics/General Atomic
P.O. Box 608
San Diego, California 92112
Attn: Librarian

General Electric Company
Atomic Power Equipment Div.
P.O. Box 1131
San Jose, California

General Electric Company
Flight Propulsion Laboratory Dept.
Cincinnati 15, Ohio
Attn: Librarian
Attn: Dr. J.W. Semmel

General Electric Company
Missile and Space Vehicle Dept.
3198 Chestnut Street
Philadelphia 4, Pennsylvania
Attn: Librarian

General Electric Company
Vallecitos
Vallecitos Atomic Lab.
Pleasanton, California
Attn: Librarian

Herring Corp.
7356 Greenback Drive
Hollywood, California 91605
Attn: Don Adams

General Dynamics/Fort Worth
P.O. Box 748
Fort Worth, Texas
Attn: Librarian

General Motors Corporation
Allison Division
Indianapolis 6, Indiana
Attn: Librarian

Hamilton Standard
Div. of United Aircraft Corp.
Windsor Locks, Connecticut,
Attn: Librarian

Hughes Aircraft Company
Engineering Division
Culver City, California
Attn: Librarian

Lockheed Missiles and Space Div.
Lockheed Aircraft Corp.
Sunnyvale, California
Attn: Librarian

Marquardt Aircraft Co.
P. O. Box 2013
Van Nuys, California
Attn: Librarian

The Martin Company
Baltimore 3, Maryland
Attn: Librarian

The Martin Company
Nuclear Division
P.O. Box 5042
Baltimore 20, Maryland
Attn: Librarian

Martin Marietta Corp.
Metals Technology Laboratory
Wheeling, Illinois

Massachusetts Institute of Technology
Cambridge 39, Massachusetts
Attn: Librarian

Materials Research and Development
Manlabs Inc.
21 Erie Street
Cambridge **39**, Massachusetts

Materials Research Corporation
Orangeburg, New York
Attn: Librarian

McDonnell Aircraft
St. Louis, Missouri
Attn: Librarian

MSA Research Corporation
Callery, Pennsylvania
Attn: Librarian

North American Aviation
Los Angeles Division
Los Angeles **9**, California
Attn: Librarian

National Research Corp.
Metals Division
45 Industrial Place
Newton, Massachusetts 02164
Attn: Dr. M. L. Torte
Director of Metallurgical Research

Lawrence Radiation Laboratory
Livermore, California
Attn: Dr. James Hadley
Head, Reactor Division

Pratt & Whitney Aircraft
400 Main Street
East Hartford 8 Connecticut
Attn: Librarian

Republic Aviation Corporation
Farmingdale, Long Island, New York
Attn: Librarian

Solar
2200 Pacific Highway
San Diego 12, California

Southwest Research Institute
8500 Culebra Road
San Antonio 6 Texas
Attn: Librarian

Rocketdyne
Canoga Park, California
Attn: Librarian

Superior Tube Co.
Norristown, Pennsylvania
Attn: Mr. A. Bound

Sylvania Electric Products, Inc.
Chem. & Metallurgical
Towanda, Pennsylvania
Attn: Librarian ,

Temescal Metallurgical
Berkeley, California
Attn: Librarian

Union Carbide Stellite Corp.
Kokomo, Indiana
Attn: Librarian

Union Carbide Metals
Niagara Falls, New York
Attn: Librarian

Union Carbide Nuclear Company
P. O. Box X
Oak Ridge, Tennessee
Attn: X-10 Laboratory Records Department

United Nuclear Corporation
Research & Engineering Center
Grassland Road
Elmsford, New York **10523**
Attn: Librarian
Attn: Mr. Albert Weinstein



Universal Cyclops Steel Corp.
Refractomet Division
Bridgeville, Pennsylvania
Attn: C. P. Mueller

TRW Space Technology Laboratories
One Space Park
Redondo Beach, California
Attn: Librarian

University of California
Lawrence Radiation Lab.
P. O. Box 808
Livermore, California
Attn: Librarian

University of Michigan
Department of Chemical & Metallurgical Eng.
Ann Arbor, Michigan
Attn: Librarian

Vought Astronautics
P.O. Box 5907
Dallas 22, Texas
Attn: Librarian

Wolverine Tube Division
Calumet & Hecla, Inc.
17200 Southfield Road
Allen Park, Michigan
Attn: R.C. Cash

Wyman-Gordon Co.
North Grafton, Massachusetts
Attn: Librarian

Wah Chang Corporation
Albany, Oregon
Attn: Librarian

Lawrence Radiation laboratory
P.O. Box 808
Livermore, California 94551
Attn: Richard R. Vandervoort